Impact of introducing electric vehicles on ground-level O₃ and PM₂.₅ in the Greater Tokyo Area: Yearly trends and the importance of changes in the Urban Heat Island effect

Hiroo Hata[1], Norifumi Mizushima[2], Tomohiko Ihara[3]

[1] Research Institute of Science for Safety and Sustainability, National Institute of Advanced Industrial Science and Technology (AIST), 16-1 Onogawa, Tsukuba, Ibaraki 305-8569, Japan
[2] Research Institute for Energy Conservation, National Institute of Advanced Industrial Science and Technology (AIST), 1-2-1 Namiki, Tsukuba, Ibaraki 305-8564, Japan
[3] Department of Environment Systems, Graduate School of Frontier Sciences, The University of Tokyo, 5-1-5 Kashiwanoha, Kashiwa, Chiba 277-8563, Japan

Correspondence to: Hiroo Hata (hata-hiroo@aist.go.jp)

Abstract. Battery electric vehicles (BEVs) are considered a solution for global warming and air pollution, and several countries have announced they will shift to BEVs in the 2030s. Even though previous studies have shown the effects of reducing vehicular emissions on the formation of tropospheric ozone (O₃), no studies have evaluated the effect of decreasing anthropogenic heat, which is expected to mitigate urban heat island (UHI) effect, on air quality issues. We used a numerical weather prediction to estimate changes in the UHI effect in the Greater Tokyo Area (GTA) of Japan by introducing BEVs. The results indicated that the introduction of BEVs would lead to a maximum local temperature decrease of 0.25 °C in the GTA. The effects of introducing BEVs on O₃ and fine particulate matter (PM₂.₅) were estimated using a regional chemical transport model. The results indicated that mitigating the UHI effect would lead to a reduction in ground-level O₃ formation. This is due to the increased NO-titration effect caused by the lowered planetary boundary layer height, and due to the degradation of photochemistry related to O₃ formation caused by a decrease in temperature and biogenic volatile organic compounds (BVOC). The mitigation of UHI would result in enhanced particle coagulation, with an increase in ground-level PM₂.₅. Furthermore, a decrease in BVOC emissions would result in increased PM₂.₅ owing to enhancement of the OH + SO₂ reaction. A total number of 175 and 77 annual premature deaths would be prevented from changes in O₃ and PM₂.₅, respectively.

1 Introduction

Climate change has significantly impacted global temperatures, inducing natural hazards and health problems (Heidari and Pearce, 2016; Dubash et al., 2018; Iacobuta et al., 2018; Fox et al., 2019). In response, worldwide organizations are attempting to restrict greenhouse gas (GHG) emissions, with the target of minimizing the temperature increase from the era of the industrial revolution to only 1.5 °C or 2.0 °C by 2100 (Fawzy et al., 2020; Schreyer et al., 2020; Strapason et al., 2020). Governments, particularly those in developed countries, have set future scenarios with the goal of achieving net zero-carbon

societies. The transport sector is known to be a large GHG emission source; thus, the introduction of battery electric vehicles (BEVs) is considered a solution for minimizing the emissions (Moro and Lonza, 2018; Shen et al., 2019; Andersson and Börjesson, 2021). The introduction of BEVs is also expected to decrease the emissions of primary air pollutants from engine exhaust and the evaporation of gasoline (Soet et al., 2014; Ferero et al., 2016; Requia et al., 2018). The nitrogen oxide (NO_X) and volatile organic compounds (VOCs) emitted by vehicles are precursors of tropospheric ozone (O_3) and fine particulate matter ($PM_{2.5}$), which are harmful to animals, including humans (Finlayson-Pitts and Pitts Jr., 1993; Sillman, 1999; Volkamer et al., 2006; Holmes, 2007), and the introduction of BEVs is expected to decrease these precursors. However, although direct exhaust emissions would be decreased, previous work suggested that the power demand would increase due to BEV battery charging (Muratori, 2018), which suggests an increase in emissions of primary air pollutants from power plants attributable to the introduction of BEVs. Nevertheless, anthropogenic heat (AH) from vehicles is expected to decrease through introducing BEVs, as engine exhaust emissions would be reduced, contributing mitigation of urban heat island (UHI) effect. Further, the UHI affects air pollutants through the following, all of which are correlated with each other: (1) changes in the kinetics of O_3 and $PM_{2.5}$ formation, (2) changes in the air mixing ratio arising from the change in ambient temperature, and (3) changes in biogenic VOC (BVOC) emissions (Ulpiani, 2021). Therefore, obtaining detailed information about how the introduction of BEVs would likely contribute to atmospheric pollution is particularly important for determining future governmental strategies.

The Greater Tokyo Area (GTA) of Japan has a large population and associated intense human activities; as such, air pollution from road traffic is a major concern. Hata and Tonokura conducted chemical transport modeling in the GTA to evaluate how ground-level O_3 concentrations change in response to the introduction of zero-emission vehicles (Hata and Tonokura, 2019). The study revealed ground-level O_3 increases in urban areas that were due to VOC-limited atmospheric conditions and the NO-titration effect (Santiago et al., 2022), and concluded that the health risk associated with increased O_3 surpasses that of influenza and heatstroke. An evaluation of the impact of nighttime BEV battery charging on ground-level O_3 by Kayaba and Kajino during the summer season in the GTA implied a non-negligible impact on the O_3 concentration (Kayaba and Kajino, 2023). However, despite the impactful findings surrounding the introduction of BEVs on the air quality in the GTA, the study only targeted O_3 as a secondary air pollutant and the evaluation of $PM_{2.5}$ was neglected, although the potential health risk of $PM_{2.5}$ is expected to be equal to or higher than O_3 (Poppe III et al., 2002; WHO Regional Office for Europe, Copenhagen, 2008). Some studies have also reported positive effects from introducing BEVs on local O_3 and $PM_{2.5}$, based on the results of chemical transport modeling (Li et al., 2016; Pan et al., 2019; Lin et al., 2020).

With respect to the UHI effect, Xie et al. (2016) conducted a model calculation to evaluate the effect of AH on ground-level O_3 in southern China, with results showing a high impact on O_3 formation, corresponding to a 2.5 ppb increase. Other studies have also indicated a positive correlation between O_3 and the UHI effect (Stathopoulou et al., 2008; Wang et al., 2018; Ulpiani, 2021). It is expected that the introduction of BEVs will decrease the local UHI effect by reducing AH (Li et al., 2015). However, despite these findings, the effects of changes in AH attributed to the introduction of BEVs on ground-level O_3 and $PM_{2.5}$, which ultimately alter the urban heat island (UHI) effect, have not been considered. Thus, a more accurate evaluation of the impact of introducing BEVs on the local air quality that considers changes in the UHI is required to assist in policymaking.

65 Therefore, the aim of this study was to determine the annual impact from the introduction of BEVs on ground-level O_3 and $PM_{2.5}$ while also examining the effect of the mitigating the UHI effect on O_3 and $PM_{2.5}$ production in the GTA. The impact of changes to the UHI resulting from the introduction of BEVs on the formation of the two atmospheric pollutants was evaluated using a chemical transport model coupled with numerical weather prediction, and a detailed analysis of the changes in ground-level O_3 and $PM_{2.5}$ was conducted within the scope of atmospheric chemistry. Finally, the change in premature mortality in

70 the GTA due to the introduction of BEVs was estimated as a representative health risk. To the best of our knowledge, this is the first study to use a chemical transport model to consider the UHI effect (relating to a shift in the use of BEVs for road transportation) on O_3 and $PM_{2.5}$. Although the target region of this study is the GTA in Japan, the results are expected to be applicable to other megacities, and can thus contribute to policymaking worldwide.

2 Methodology

75 **2.1 Scenarios for replacing internal combustion vehicles with battery electric vehicles (BEVs)**

The aim of this study was to assess the effect of replacing internal combustion vehicles (ICVs) with BEVs. Nine categories of vehicles were considered in the emissions inventory within this study: light and normal passenger cars (PV), buses, light and small tracks (TV), heavy-duty vehicles (HV), motorcycles, and vehicles used for specific purposes (Shibata and Morikawa, 2021). The worldwide strategy to mitigate GHG reduction focuses on the complete substitution of ICVs with BEVs over the

80 period 2030 to 2035 (Mulrow and Grubert, 2023), with net zero emissions from all vehicles by 2050. Owing to technological issues relating to the capacity of batteries used in BEVs, it remains unclear whether HVs can be completely electrified (Forrest et al., 2020), and several plans have suggested introducing renewable fuels instead of providing electrification for these vehicles (Hosseinzadeh-Bandbafha et al., 2021). Therefore, in this study, BEV replacement concentrated only on PVs and TVs. The electrification strategy for motorcycles and specific purpose vehicles is unclear, and the impact of these vehicles on air

85 pollution is expected to be lower than that of other vehicles in Japan; thus, the electrification of these vehicles was also not included in the study.

2.2 Numerical Weather Predictions

2.2.1 General information

A Weather Research and Forecasting Model (WRF v4.3.3) was used to obtain meteorological conditions (Skamarock et al.,

90 2024) from Dec. 1, 2016 to Dec. 31, 2017. The first month was treated as the spin-up period and the whole of 2017 as the analysis period. Figure 1 shows the calculated domains: East Asia (D1: 45×45 km), Japan (D2: 15×15 km), and the GTA (D3: 5×5 km).
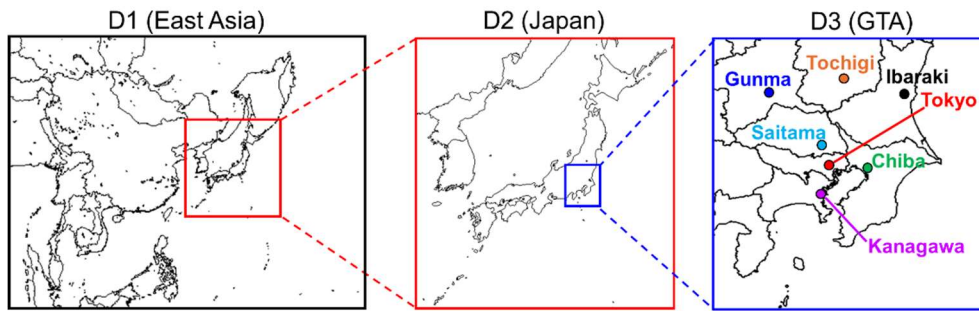
Figure 1: Domains used for numerical weather prediction and the chemical transport model. Seven prefectural areas in the Greater Tokyo Area are highlighted in domain D3.

Objective analysis data describing the initial and boundary conditions were obtained at a resolution of 1° × 1° from the FNL Final Operational Global Analysis data provided by the National Center for Atmospheric Research (NCAR: National Center for Atmospheric Research archives, 2024). The boundary conditions of sea surface temperature for 0.082° × 0.082° were obtained from the National Oceanic and Atmospheric Administration (NOAA) (Environmental Modeling Center Archives, 2024). The simulation results were validated through a comparison with observation data from the Japan Meteorological Agency (Japan Meteorological Agency archives, 2024). Seven sites, the metropolitan areas of Tokyo (urban), Kanagawa (urban), Chiba (urban), Saitama (urban), Tochigi (suburban), Gunma (suburban), and Ibaraki (suburban/rural) were selected to represent urban and suburban/rural areas, respectively, and the details of these are listed in Table S1 of the supporting information (SI). A single-layer Urban Canopy Model (UCM: Kusaka et al., 2021) was combined with the WRF calculations so that the UHI effect before and after the introduction of BEVs could be considered. UCM parameters obtained from a previous study (Hara et al., 2010) were used to determine the urban canopy parameters for the GTA. Highlighting the UCM parameters related to AH, Hara et al. provided maximum AH as 29.0 W m^{-2} at 18:00 and 19:00 for three urban area category types (low-density residential, high-density residential, and commercial areas), and this is reflected in the anthropogenic heating diurnal profile of the GTA shown by the black square dots in Fig. 2. Further details of the simulation setup for the WRF are listed in Table S2 of the SI. Validation of observed and simulated meteorology are discussed in Appendix C.
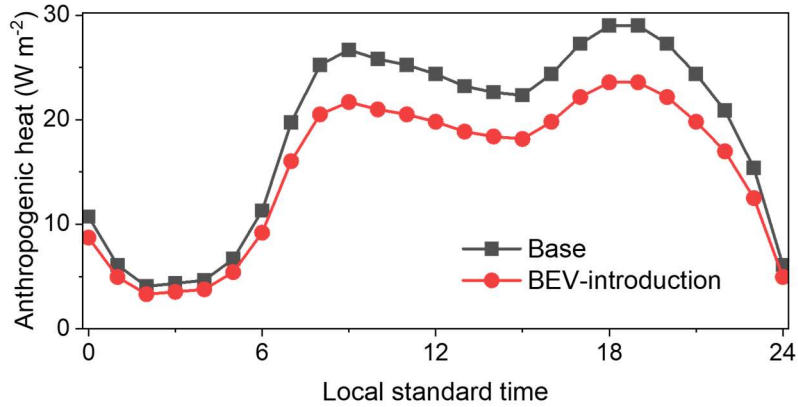
Figure 2: Diurnal changes in anthropogenic heat throughout a 24 h period set in this study. Black square dots represent the base case and red circle dots represent the BEV-introduction scenario.

2.2.2 Consideration of UHI effects after the introduction of BEVs

Several studies have suggested that the UHI is one of the results of AH associated with transportation (Rosenfeld et al., 1998; Nuruzzaman, 2015; Rizvi et al., 2023), and that the introduction of BEVs is expected to eradicate this issue. The changes in the total energy efficiency of BEVs compared to ICVs affects AH as well as vehicular exhaust emissions, leading to local changes in the UHI. The process used to evaluate AH following the introduction of BEVs is described in Appendix A. Briefly, two categories of passenger cars and one small truck were treated as model vehicles in this study (Tables A1 and A2). Using the fuel consumption for ICVs and electric consumption for BEVs obtained from catalogue data provided by the manufacturers, the differences in the energy efficiencies of ICV and BEV were calculated. Statistical data of the number of vehicles (Database from Automobile Inspection & Registration Information Association, 2024), average mileage per year (Ministry of Land, Infrastructure, Transport, and Tourism, 2024), and the heat enthalpy of gasoline and light fuel (Agency for Natural Resources and Energy, 2024) were then applied, and the total AH produced by ICVs and BEVs was calculated. Data describing stationery and transportation sources in Tokyo in 2010 (Ministry of the Environment, 2024) were used to calculate the AH from these sources. The results showed a reduction ratio of 0.813 or 18.7 % for AH in the GTA through the introduction of BEVs. Therefore, the value of 0.813 was multiplied by 29.0 W m^{-2}, which is the maximum value of AH proposed by Hara et al. (2010), and a value of 23.6 W m^{-2} was derived for AH associated with the BEV-introduction scenario. The diurnal profile of AH in BEV-introduction scenario is described using the red circle dots in Fig. 2. Note that the UCM coupled in WRF provides only the average distribution of AH and other urban canopy parameters. In an urbanized region such as GTA, the distribution of on-road vehicles is expected to be distributed equally. Nevertheless, there is also countryside in domain D3 shown in Fig. 1 at the western, eastern, northern, and southern borders of those areas, and the applied reduction ratio might therefore be overestimated. Such a limitation is discussed later in the section. In addition, the introduction of BEVs is expected to increase AH from power plants due to the increased demand for electricity used in battery charging; however, the increased AH from

power plants was not considered in this study. Power plants in GTA are located in specific areas near the bay, and are not distributed throughout the entire area; therefore, it was difficult to consider the effect of AH from power plants and its subsequent UHI effects in the GTA.

2.3 Chemical transport modelling

2.3.1 Modelling description

A community multiscale air quality modeling system (CMAQ v5.3.3: Murphy et al., 2021) was used to calculate the air quality in Japan. The calculated domains were the same as those used in the WRF model shown in Fig. 1, and regional nesting method was applied for domain D2 (parent domain: D1) and for domain D3 (parent domain: D2). Domain D3 was the analyzed region. The dates of winter, spring, summer and autumn were as follows, respectively: Jan. 1 2017 to Mar. 31 2017, Apr. 1 2017 to June 30 2017, Jul. 1 2017 to Sep. 30 2017, and Oct. 1 2017 to Dec. 31 2017. The meteorological inputs obtained from the results of the WRF calculations described in Section 2.2 were applied to the CMAQ calculation. SAPRC-07 was used to describe the gas-phase chemical mechanism (Carter, 2010), and the AERO6 module with ACM liquid chemistry was used as the aerosol chemical mechanism (Binkowski and Roselle, 2003). The emission inventories were provided by Chatani et al. (Chatani et al., 2018) and are briefly summarized as follows. Hemispheric Transport of Air Pollution (HTAP) v2.2 (anthropogenic emissions: Janssens-Maenhout et al., 2015), Global Fire Emissions Database (GFED) v4.1 (biomass burning: van der Werf et al., 2017), AeroCom (volcanos: Diehl et al., 2012), and Model of Emission of Gases and Aerosols from Nature (MEGAN) v2.1 for (BVOC emissions: Guenther et al., 2012) were applied for emissions outside of Japan (D1). The Japan Clean Air Program (JCAP)/Japan AuTo Oil Program (JATOP) Emission Inventory for Vehicle Emission Model (JEI-VEM) (vehicular emissions: Chatani et al., 2011; Shibata and Morikawa, 2021), the Sasakawa Peace Foundation (ship emissions: Sasakawa Peace Foundation, 2022), Japan Meteorological Agency (volcanos: Japan Meteorological Agency, 2022), and MEGANv2.1 (BVOC emissions: Guenther et al., 2012) were applied for emissions inside Japan (D2 and D3). The results of chemical transport modeling were validated by comparing the seven observation sites listed in Table S1, and the details are discussed in Appendix C. The primary emissions, evaporative VOC emissions, and refueling processes associated with the use of ICVs were expected to decrease under the introduction of BEVs; however, charging batteries increases the requirement for energy from power plants, increasing the emissions from this source.

2.3.2 Emission changes resulting from the substitution of ICVs with BEVs

Three categories of vehicular emissions affect the environment: tailpipe engine exhaust emissions (both hot- and cold-start emissions), evaporative emissions from gasoline fleets (hot soak, diurnal breathing, and running losses), and particulate dust from tires (break, tire, and hoisting dust) (Shibata and Morikawa, 2021). Stationary sources, such as VOC emissions during refueling (Yamada et al., 2018) and power plants that supply energy for battery charging (Casals et al., 2016; Kayaba and Kajino, 2023a) also require consideration. In the BEV-introduction scenario, all exhaust, evaporative, and refueling emissions

from the targeted vehicles were set to zero. Changes in particulate dust emissions were not considered in this study, although a previous study suggested that brake dust would increase after the introduction of BEVs owing to the weight of the battery (Kayaba and Kajino, 2023b). The increase in primary emissions from power plants due to charging BEVs was estimated using the value of the charging voltage of specific electric vehicles, as described in Sect. A1 of Appendix A. The results suggested a 33.8 % increase in the amount of air pollutants from power plants for the GTA.

2.3.3 Scenarios for the chemical transport model

Details of the two major scenarios investigated in this study (BASE, a basic scenario without the introduction of BEVs, and ALL, BEV-introduction scenario) are listed in Table 1. The ALL scenario considers the effects of introducing BEVs and includes emission reductions from engine exhausts (anthropogenic VOCs (AVOCs), particulate matter (PM), ammonia (NH_3), sulfur dioxide (SO_2), and carbon monoxide (CO)), evaporative emissions (AVOCs), emission increases from power plants (NO_X, PM, SO_2, and CO) as a result of battery charging, and UHI changes. Four sensitivity scenarios (the introduction of BEVs (S_{EV}), the increase in emissions from power plants (S_{PP}), the change in ambient temperature (S_{UHI}), and the change in BVOC emissions resulting from changes to the UHI (S_{BVOC})) were also examined to evaluate the contributions of emission reductions to the formation of ground-level O_3 and $PM_{2.5}$ in the GTA. Note that S_{UHI} only considered the effects of temperature change, and that the change in BVOC emissions due to such temperature changes was not included. The BASE scenario was calculated for D1, D2, and D3, while all other scenarios were calculated only for the D3 domain using the initial and boundary conditions obtained from the BASE scenario. Changes in the annual mean primary NO_X, AVOCs, PM, NH_3, SO_2, and BVOC emissions for the scenarios listed in Table 1 are also shown in Figs. B1 to B4 of Appendix B as well as the distribution of changes in emissions described in Figs. S1 to S4 of the SI.

Table 1: Six scenarios calculated using the chemical transport model.

Scenario	Definition
BASE	Base scenario for 2017.
ALL	Includes total effects of substituting ICVs with BEVs.
S_{EV}	Sensitivity scenario clarifying the effect of reducing engine exhaust and evaporative emissions.
S_{PP}	Sensitivity scenario clarifying the effect of increasing power plant emissions.
S_{UHI}	Sensitivity scenario clarifying the effect of changes in temperature as a result of AH reduction.
S_{BVOC}	Sensitivity scenario clarifying the effect of changes in BVOC emissions caused by the change in temperature.

3 Results

3.1 UHI effect in the GTA

190 Figure 3 shows the average difference in the ground surface temperature (ΔT) between the BASE and ALL cases over four seasons as calculated using the WRF. The seasonal ΔT distributions are described in Fig. S5 of the SI. According to Fig. 3(a), a decrease in the average ΔT in the calculated domain is due to the decrease in AH resulting from the introduction of BEVs. According to Fig. S5, the decrease in ΔT is high in winter and autumn and low in summer, and is distributed from the center of Tokyo, where high AH is expected as a result of condensed anthropogenic activity. The seasonal changes in ΔT for the

195 seven prefectures of the calculated domain D3 described in Fig. 1 were extracted and are presented in Fig. 3(b), which show a range of -0.1 – -0.25 °C for ΔT, with relatively high error bars, particularly for spring and summer. This is likely because of the high planetary boundary layer (PBL) that forms in the warmer seasons, which enhances thermal convection and leads to the large discrepancies observed in the ΔT. The change in the PBL height between the ground surface and the free troposphere due to the change of the UHI effect is described in Fig. S6 of the SI. According to Fig. S6 (a)–(c), the PBL height decreased

200 by ~3% in the winter, spring, and summer seasons, but the change in the PBL height reached ~30% in autumn. The change in the UHI effect is expected to affect air pollution via atmospheric conditions (changes in the rate constants of atmospheric chemical reactions and changes in the mixing ratio of air due to the change of PBL height) and emissions (BVOC emissions from biogenic sources). These effects are discussed in the later Sects. 4.1 and 4.2.
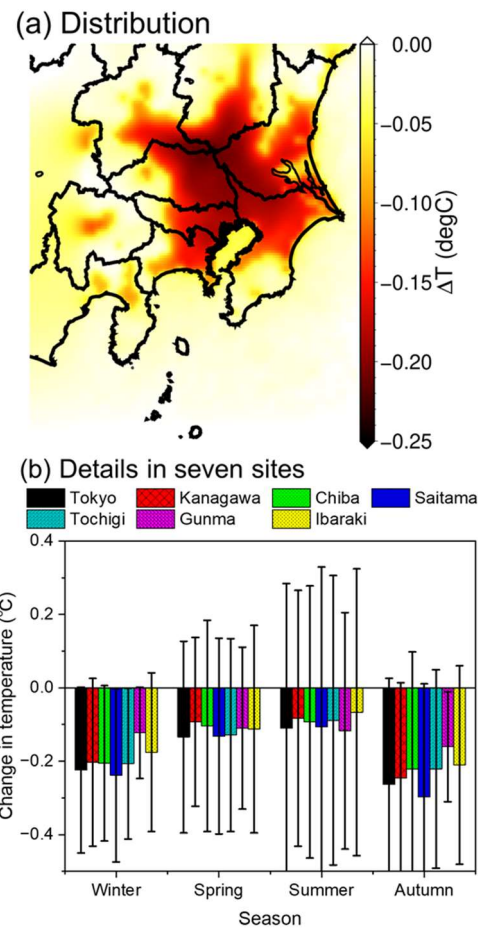
Figure 3: Changes in ground temperature following the introduction of battery electric vehicles in the Greater Tokyo Area: (a) yearly averaged distribution, and (b) seasonal variation in seven prefectures.

3.2 Effect of introducing BEVs on ground-level O_3 and $PM_{2.5}$ concentrations

3.2.1 Overall effects

Figure 4 shows the overall effects of introducing BEVs on changes in yearly averaged O_3 and $PM_{2.5}$ concentrations within the GTA, which were evaluated using the difference between the results of the ALL and BASE scenarios. As shown in Fig. 4(a), O_3 increased around the central area of the GTA, as well as in several other sites; these results are consistent with those of previous studies (Hata et al., 2019; Kayaba and Kajino, 2023a). The seasonal changes in O_3 are shown in Fig. S7 of the SI. The results show that a strong increase in O_3 was estimated in the winter and autumn seasons, associated with a considerable decrease in temperature related to the reduction in the UHI effect discussed in Section 3.1. However, a slight increase in O_3 in the spring and summer seasons indicated that the UHI effect contributed significantly to local O_3 formation in the winter and autumn seasons. According to Fig. 4(b), increases in $PM_{2.5}$ also occurred on the western and northern sides of the GTA.

However, as primary PM$_{2.5}$ emissions are expected to decrease as a result of introducing BEVs; this increase was attributed to the enhanced formation of secondary aerosols. Seasonal changes in PM$_{2.5}$ are shown in Fig. S8 of the SI.
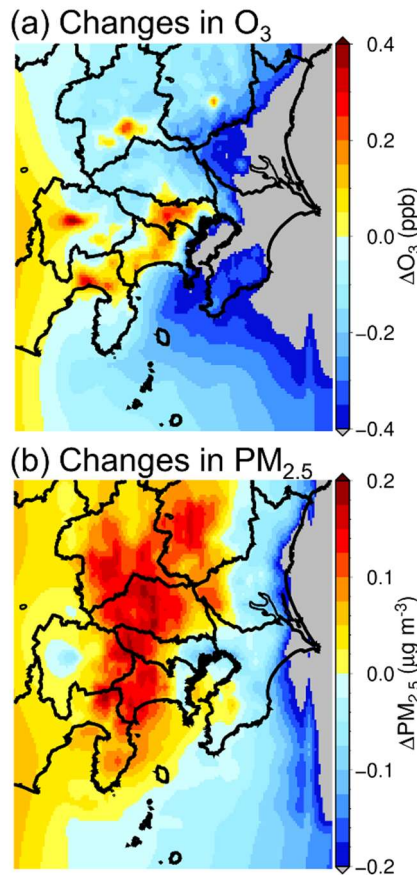
Figure 4: Changes in the yearly-averaged (a) O$_3$ and (b) PM$_{2.5}$ concentrations following the introduction of battery electric vehicles (BEVs) in the Greater Tokyo Area. Results include the effects of all BEV-introduction (ALL scenario), including the reduction of primary air pollutants from the transport sector, the increase in the primary air pollutants due to the high energy demands of battery charging, urban heat island (UHI) mitigation, and changes in the BVOC emissions as a result of UHI mitigation.

3.2.2 Sensitivity analysis of changes in O$_3$

The contributions of the five scenarios that were subtracted from the BASE scenario (ALL, S$_{EV}$, S$_{PP}$, S$_{UHI}$, and S$_{BVOC}$) to changes in the O$_3$ concentrations in Tokyo and Tochigi are shown in Fig. 5. Tokyo was chosen as the representative urban site and Tochigi as the representative suburban site. The results of Kanagawa, Chiba, Saitama, Gunma, and Ibaraki are described in Fig. S9 of the SI. Detailed definitions of the scenarios are described in Sect. 2.3.3 and Table 1. According to Fig. 5, the seasonal trends obtained using the five scenarios were similar for Tokyo and Tochigi. As mentioned in Section 3.2.1, the results of ALL showed an increase in O$_3$ during winter and autumn and decreases in spring and summer, with S$_{EV}$ also showing a decrease in O$_3$ for the summer season in Tokyo and Tochigi. According to a previous study (Kayaba and Kajino, 2023a), atmospheric conditions in the urban area of the GTA are VOC-limited during summer; thus, the reduction in NO$_X$ from

vehicular emissions led to an increase in O_3 in Tokyo and Tochigi. The regime analyses in Section 4.1.1 presents the ozone sensitivity regime in seasons other than the summer. The S_{PP}, S_{UHI}, and S_{BVOC} scenarios indicate negative impacts on O_3 formation in Tokyo and Tochigi in all seasons. The increase in air pollutants from power plants, mainly NO_X, led to an NO-titration effect, which lowered the O_3 concentration in Tokyo and Tochigi. The power plants are located in the bay area around Tokyo, and a detailed map of these is provided in a previous study (Kayaba and Kajino, 2023a). Notably, the mitigation effect of the UHI caused a significant decrease in O_3 formation within Tokyo, which was attributed to the kinetics of a lowered PBL height and the photochemistry of O_3 formation, details of which are discussed in Sections 4.1.2 and 4.1.3, indicating the importance of introducing BEVs to mitigate O_3 problems in urban areas, not only in terms of direct emissions but also with respect to the local temperature decrease. The UHI effect was lower in Tochigi than it was in Tokyo because Tochigi is a suburban site, as seen in Fig. 3. Mitigation of the UHI effect also caused a decrease in BVOC emissions in central GTA and an increase on the west side of the GTA. BVOCs have a high O_3-formation potential; thus, the decrease in BVOC emissions in the center of the GTA reduced the O_3 concentrations in Tokyo and Tochigi. The results of the S_{UHI} and S_{BVOC} scenarios indicated that the introduction of BEVs mitigated the UHI effect, leading to deactivation of both O_3 formation and BVOC emissions.
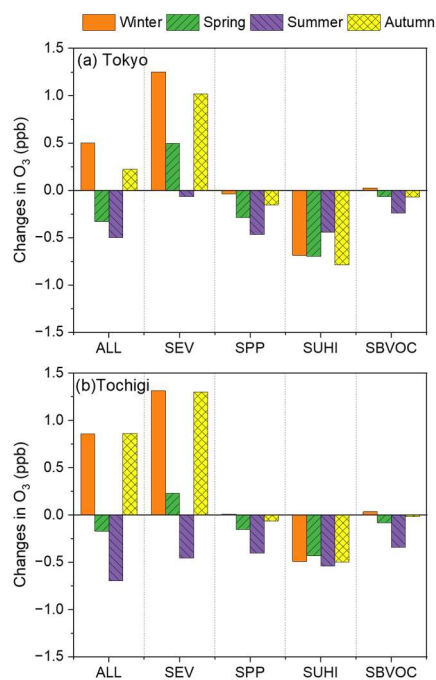
Figure 5: Contributions of the five scenarios listed in Table 1 to the changes in O_3 in the Greater Tokyo Area in (a) Tokyo and (b) Tochigi.

3.2.3 Sensitivity analysis of changes in PM₂.₅

Figure 6 shows the contributions of the five scenarios (ALL, S_{EV}, S_{PP}, S_{UHI}, and S_{BVOC}) to the changes in the PM₂.₅ concentration in Tokyo and Tochigi. The results of Kanagawa, Chiba, Saitama, Gunma, and Ibaraki are described in Fig. S10 of the SI. Unlike O₃, the seasonal trends in Tokyo and Tochigi showed different behaviors. The S_{EV} scenario negatively or slightly affected PM₂.₅, owing to the decrease in primary emissions from the exhaust emissions. S_{PP}, S_{UHI}, and S_{BVOC} caused an increase in PM₂.₅ in both Tokyo and Tochigi over most of the year. Overall, unlike O₃, UHIs positively affect PM₂.₅ formation, and changes to the UHI are likely to have negative effects on the GTA.
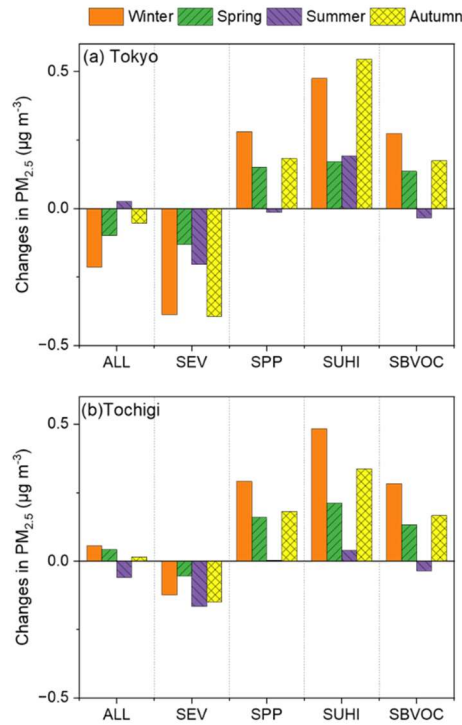
Figure 6: Contributions of the five scenarios listed in Table 1 to the changes in PM₂.₅ in the Greater Tokyo Area in (a) Tokyo and (b) Tochigi.

The annual distributions of the four components of PM₂.₅, $NO_3^-(p)$, $SO_4^{2-}(p)$, $NH_4^+(p)$, and secondary organic aerosols (SOA) for the four sensitivity scenarios are shown in Fig. 7. In terms of S_{EV}, a large decrease in $NO_3^-(p)$ was estimated due to reductions in the primary emission of NO_X. However, $SO_4^{2-}(p)$ increased because of the increased O₃ level, enhancing OH formation and increasing the $SO_4^{2-}(p)$ attributed to the SO_2 + OH reaction. Increases in $SO_4^{2-}(p)$ enhance SOA formation, leading to a large increase (Budisulistiorini et al., 2017). The sensitivity scenario of S_{UHI} showed an increase in all components. It is well known that $NO_3^-(p)$ is in equilibrium with $HNO_3(g)$ in the atmosphere, and that the equilibrium shifts to the $NO_3^-(p)$ form when the temperature increases, which is why a strong increase in $NO_3^-(p)$ occurred in the S_{UHI} sensitivity scenario (Morino et al., 2006). The decrease in temperature resulting from the introduction of BEVs in the S_{UHI} scenario enhanced the

condensation of SOA, leading to an increase in the remaining components (Sheehan and Bowman, 2001). The S_{BVOC} scenario
270 showed an increase in the components of PM$_{2.5}$. Since no temperature change was considered in the S_{BVOC} scenario, an increase
in PM$_{2.5}$ was not expected while changes in the UHI led to changes in the amount of BVOC emissions in the S_{BVOC} scenario.
According to Fig. S4, BVOC emissions decreased owing to changes in the UHI effect in some regions, where an increase in
the SO$_4^{2-}$(p) was observed, as seen in Fig. 7. This was unexpected because BVOCs are considered to be precursors of OH,
which contributes to SO$_4^{2-}$(p) formation via reaction of SO$_2$ + OH; the possible reasons for this are discussed in Section 4.2.
275 The S_{EV} scenario also assumed the reduction in primary emissions from vehicles, meaning that a decrease in SO$_4^{2-}$(p) was
expected. Nevertheless, all components of PM$_{2.5}$, especially SO$_4^{2-}$(p) and SOA, were observed to increase considerably in the
western and northern areas of the GTA, corresponding with the suburban to rural areas.
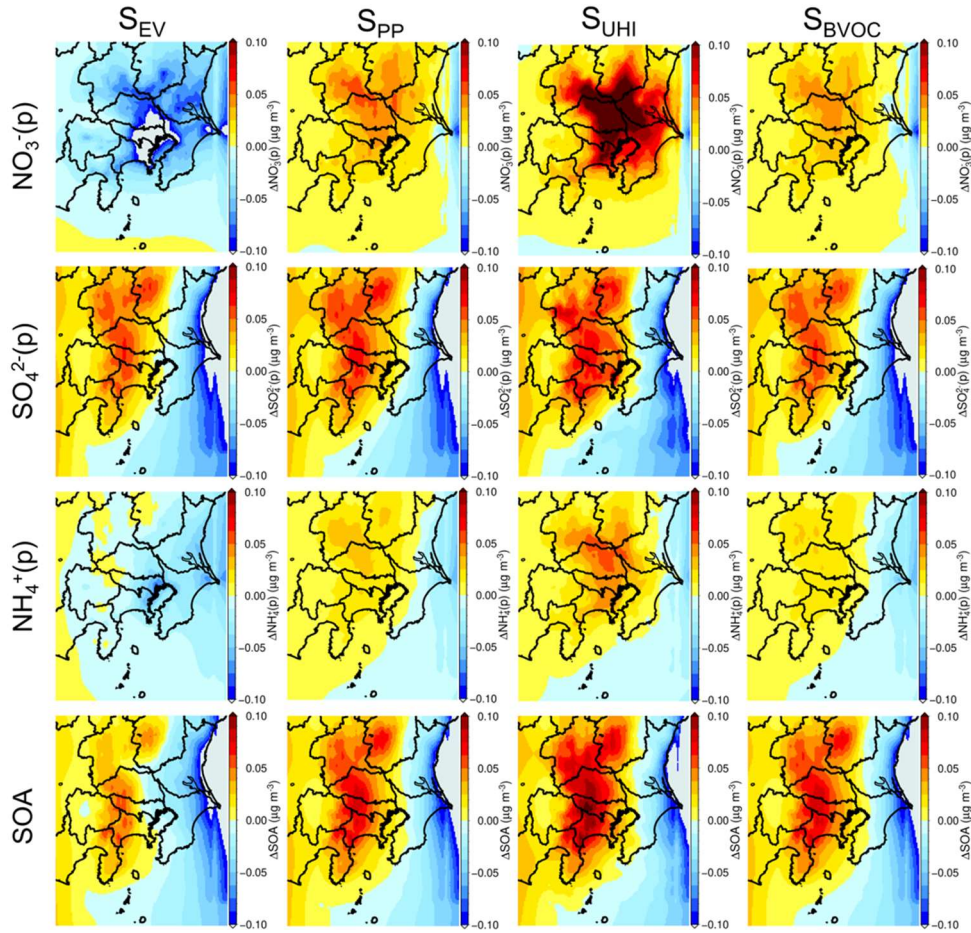
Figure 7: Contributions of the four sensitivity scenarios listed in Table 1 to the annual average PM$_{2.5}$ composition in the Greater
280 **Tokyo Area.**

4 Discussion

4.1 Analysis of the reason for changes in ground-level O_3 concentrations

4.1.1 Analysis of ozone formation sensitivity regime in the GTA

Figure 8 shows the seasonal average of the hydrogen peroxide (H_2O_2) to HNO_3 ratio (HNR) for the four seasons, each of which
was averaged from 09:00 to 15:00 to represent the sensitivity of daytime photochemical O_3 formation. Details of the HNR and
related topics of O_3 formation-sensitive regimes are described in Appendix D. According to Fig. 8, the HNR values around
Tokyo were less than 0.5 for all seasons, meaning that the central Tokyo region of the GTA is VOC-sensitive throughout the
year. A relatively wide distribution of VOC-sensitive regimes was observed in spring, summer, and autumn, whereas a narrow
distribution was observed in the winter. According to Section 3.2.1 and 3.2.2, the sensitivity of introducing BEVs (scenario
S_{EV}) to O_3 formation showed positive effects in winter and autumn. The value of ~0.1 for the HNR in Tokyo in winter and
autumn indicates strong VOC sensitivity in Tokyo, and the decrease in the NO_X might surpass the effect of the VOC reduction,
resulting in an increase in O_3 in the S_{EV} scenario for those seasons. Despite this, the degradation in the O_3 formation that results
from the mitigation of the UHI effect contributed to reducing the effect of the increase in O_3, resulting in a mild increase in O_3
under the ALL scenario in winter and autumn. However, according to Fig. 8(b) and (c), the HNR was close to 0.5 for spring
and summer, which is the border between the VOC-sensitive regime and NO_X-sensitive regime in and around central Tokyo.
According to Section 3.2.2, the S_{EV} scenario resulted in decreased O_3 formation during spring and summer. Particularly in
summer, Fig. 5 shows a decrease in O_3 under the S_{EV} scenario in both Tokyo and Tochigi, despite the fact that Tokyo and
Tochigi are VOC-sensitive and transition regimes, respectively. This means that the effect of the VOC reduction might surpass
the effect of the NO_X reduction in the warmer seasons, contributing to the decrease in O_3. Combined with the strong impact
attributed to UHI mitigation as a result of the introduction of BEVs, O_3 was estimated to significantly decrease in the warmer
seasons (ALL scenario). S_{PP}, the scenario used to confirm the effect of the increase in power plant emissions, also contributed
to the decrease in O_3, similar to UHI mitigation (S_{UHI} and S_{BVOC}). Of note, NO_X is the primary pollutant emitted by power
plants. According to Fig. 8, central GTA was mostly VOC-limited, and the increase in NO_X emissions caused a decrease in
O_3, leading to the observed decrease in O_3 in both Tokyo, Tochigi, and other regions under the S_{PP} scenario.
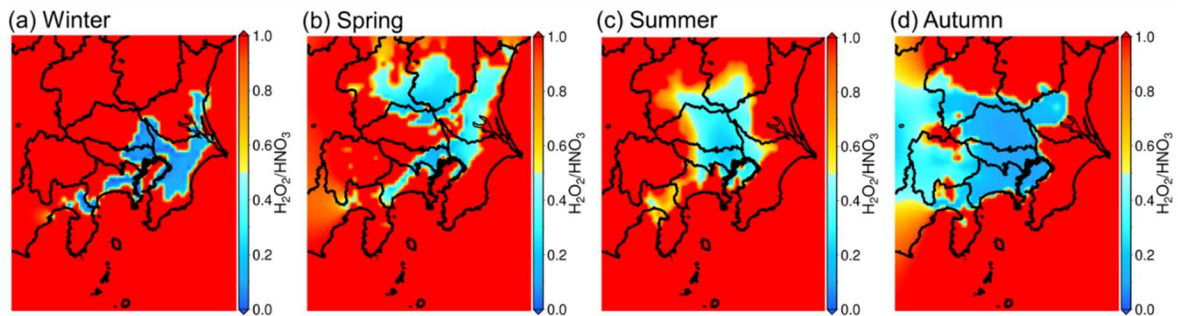
**Figure 8: Seasonal trends in the ozone sensitivity regime defined by the ratio of H_2O_2/HNO_3 (HNR) for four seasons. Analysis was
conducted by averaging the results for 09:00 to 15:00 daily. Values > 0.5 are NO_X-limited and < 0.5 are VOC-limited.**

4.1.2 Analysis of NO-titration in the GTA and the potential cause of the decrease in ground-level O_3 through the UHI effect

The effect of NO-titration is important when discussing the impact of changes in primary emissions on direct O_3 formation (Akimoto et al., 2015). The concentration of total produced O_3, or potential O_3 (PO), is defined using $[PO] = [O_3] + [TO]$. TO is the titrated-O_3 from NO-titration, and the concentration is defined by $[TO] = [NO_2]-\alpha[NO_X]$, where the parameter α is the ratio of primary NO_2 emissions to total NO_X emissions in the atmosphere. A value of 0.1 for α is widely accepted in Japan (Itano et al., 2007; Akimoto et al., 2015). Figure 9(a)–(d) shows the seasonal variations in the change in TO (ΔTO) between the BASE and S_{UHI} scenarios. The change in the NO-titration effect was strong in central Tokyo throughout the year because of high NO_X emissions and relatively high O_3 concentrations, showing high ΔTO sensitivity. Compared with the spring and summer, a wider distribution of high ΔTO was observed for winter and autumn, and more relevant NO-titration effects were estimated in these seasons; these were presumed to be caused by the intense decrease in temperature caused by mitigation of the UHI effect. Haman et al. conducted observational and CTM calculations based on Houston (U.S.) from 2008 to 2010 to clarify the relationship of diurnal temperature, PBL, and ground-level O_3 (Haman et al., 2014). The results suggested a positive relationship between ground-level O_3 and the PBL height; this was due to the enhancement of NO-titration caused by relatively weak wind speeds during the lower PBL height which caused NO_X to remain on the ground surface. Figure 9(e)–(f) shows the seasonal changes in ground-level O_3 between the BASE and S_{UHI} scenarios (ΔO_3). A higher decrease in O_3 is estimated in the central area of GTA, and winter and autumn show a high O_3 decrease; these results are also confirmed in Fig. 5. The seasonal variations in the positive increase in O_3 shown in Fig. 9(e)–(f) correspond to ΔTO shown in Fig. 9(a)–(d). However, the distributions of ΔO_3 shown in Fig. 9(e)-(f) do not correspond to the distributions of the H_2O_2/HNO_3 ratio. The results indicate that O_3 reductions caused by the mitigation of UHI effects are attributed by the enhanced NO-titration effect rather than the photochemistry involved in O_3 formation. Enhancement of the NO-titration effect contributes to a maximum decrease in O_3 of ~1.0 ppb. Despite these facts, Haman et al. suggested that the relationship between PBL and the NO-titration effect strongly depends on factors such as the regions analyzed and meteorology (Haman et al., 2014). Future work should determine the relationship between UHI effects and O_3 in other regions. The impact of the change in temperature on photochemical reactions is discussed in the next section.
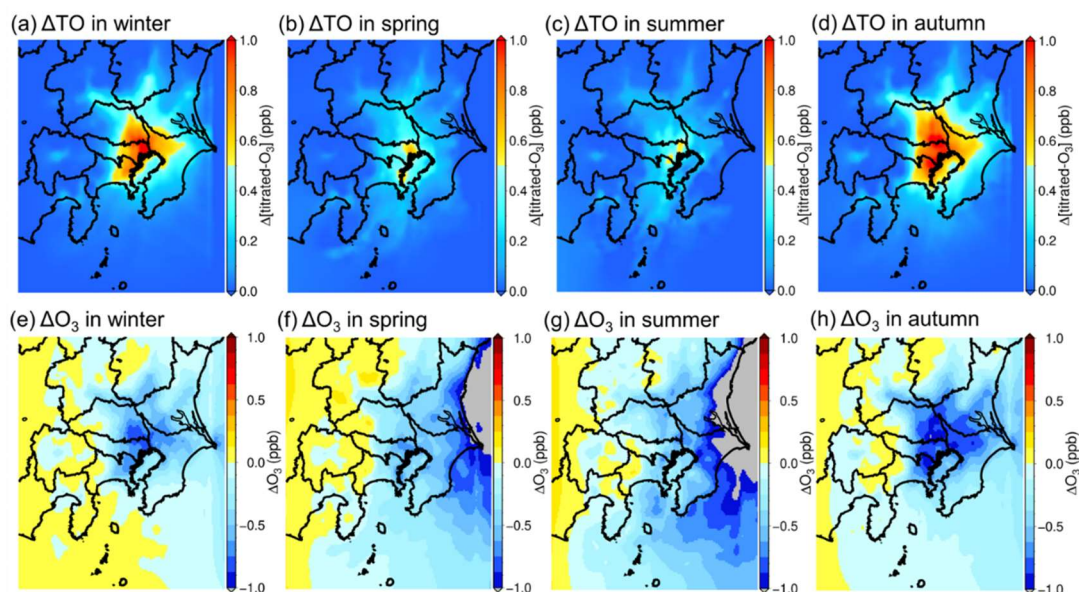
Figure 9: Seasonal trend in the effect of: (a–d) the change in O₃ reduced by NO-titration (ΔTO) between BASE and UHI scenario (S_UHI); and (e-h) the change in ground-level O₃ (ΔO₃) between BASE and S_UHI scenarios for the four seasons.

4.1.3 Box model simulation of the temperature dependence of ozone formation chemistry

Section 4.1.2 discusses the decrease in ground-level O_3 caused by the enhancement of NO-titration effect due to the lowered PBL height from mitigation of the UHI effect. Mitigation of the UHI effect causes a local-temperature decrease and is expected to weaken the rate of photochemistry involved in O_3 formation. For example, Coates et al. suggested that O_3 formation is enhanced through the increase in temperature due to the increased reaction rate of VOC oxidation and peroxy nitrate decomposition (Coates et al., 2016). Meng et al. suggested that high temperatures lead to a high HO_2 + NO reaction rate, which increases NO_2 and contributes to high O_3 episodes (Meng et al., 2023). To clarify the effect of temperature changes on the photochemistry of O_3 formation, a box model calculation using SAPRC-07 (Carter, 2010) was conducted in this study. The CO emissions were the highest in the D4 region among all primary emissions (as shown in Fig. B1 of the Appendix B) and the CO concentration was set to 1 ppm. The concentrations of the remaining pollutants, including NO_X, SO_2, AVOCs, and BVOCs, were set using the ratio between the annual amount of each emission in the BASE scenario shown in Fig. B1 to Fig. B4 and that of CO. The detail settings of the concentrations of the species for box model simulation are listed in Table S4 of the SI. The concentration of H_2O was fixed to 1.56×10^4 ppm; this was estimated from the value of partial vapor pressure of H_2O at 25 °C with 50 % relative humidity. Solar intensity was defined by J_{NO2}, which is the rate of photodissociation of NO_2 + $h\nu \rightarrow$ NO + O(^{3}P). In this study, J_{NO2} was set to 0.4 min^{-1} which is the medium value of 0.27–0.54 min^{-1} in an ambient condition within the mid-latitude region of Greece, as reported in a previous study (Gerasopoulos et al., 2012). The calculated temperature range was 0–35 °C. The black square dots in Fig. 10 shows the results of the maximum O_3 (ppm) concentration calculated using the box model. The O_3 concentration varied between 0.32 and 0.66 ppm from the calculated temperature

range, meaning that temperature is an important factor in O_3 formation. The red circle dots in Fig. 10 shows the temperature dependence of the percentage of the change of O_3 concentration per unit temperature ($d[O_3]/dT$ (%/°C)). $d[O_3]/dT$ is highest at 15 °C with the value of 3.2 %/°C. The temperature of 15 °C in Japan corresponds to the early spring and late autumn seasons. Assuming that the O_3 concentration is 50 ppb in spring and autumn seasons, the change of 3.2 (%/°C) corresponds to 1.6 ppb/°C. According to Fig. 3, mitigation of the UHI effect causes a maximum temperature decrease of 0.25 °C; therefore, the change in the O_3 concentration attributed to the photochemical reaction is roughly estimated to be 1.6 ppb/°C × 0.25 °C = 0.4 ppb. In Section 4.1.2, enhancement of the NO-titration effect was attributed to a maximum of a 1 ppb decrease in O_3, indicating that the enhancement of O_3 photochemistry contributed to less than half of that of NO-titration effect when mitigation of the UHI effect occurred through introducing BEVs in the GTA.
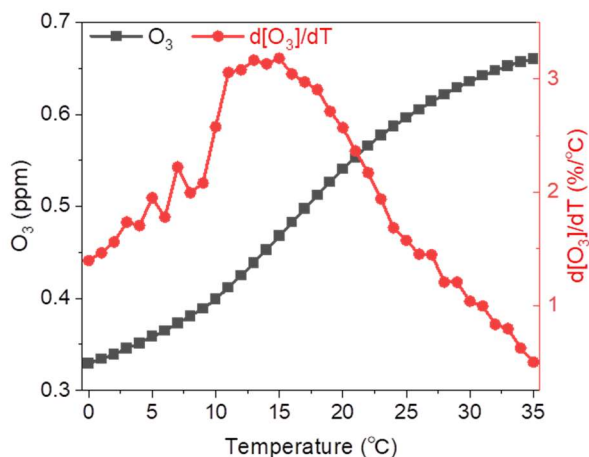
Figure 10: Temperature dependence of O_3 and percentage change in O_3 concentration per unit temperature ($d[O_3]/dT$) calculated using the box model SAPRC-07.

4.2 Correlation between PM$_{2.5}$ increase, change in BVOC emissions, and UHI effect

The sensitivity scenarios for S_{BVOC} described in Section 3.2.3 show an unreasonable increase in SO_4^{2-}(p) and a simultaneous increase in SOA. This indicates that not only the change in temperature and PBL height, but also the change in BVOC emissions caused by mitigation of the UHI effect, would lead to increases in SO_4^{2-}(p) and SOA. According to Fig. S4, a decrease in BVOC emissions would occur in some parts of the central to northern regions of the GTA, with an increase observed in other areas. Considering the change in BVOC emissions, the change in SO_4^{2-}(p) in the S_{BVOC} scenario can be explained through discussions about atmospheric chemistry that are divided into daytime and nighttime, as seen in the following sections 4.2.1 and 4.2.2.

4.2.1 Sensitivity analysis of daytime PM$_{2.5}$ changes

375 First, considering the daytime S$_{BVOC}$ scenario, the simplified oxidation reactions of BVOC and SO$_2$ are described in the following chemical reactions in which the particle formation schemes are simplified (it is of note that BVOC oxidation by O$_3$ is not considered in this discussion because the rate of oxidation by OH is much faster than that associated with O$_3$),

$$BVOC + OH \rightarrow SOA, \qquad (R1)$$

380

$$SO_2 + OH \rightarrow SO_4^{2-}(p). \qquad (R2)$$
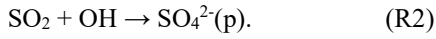
The atmospheric oxidizer OH is generated by the following photochemical reactions during the daytime,

385 $$O_3 + hv \rightarrow O_2 + O(^1D), \qquad (R3)$$

$$O(^1D) + H_2O \rightarrow 2OH. \qquad (R4)$$
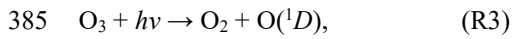
Assuming a steady-state approximation of the intermediate radicals, the rates of O(^1D) and OH are described by Eqs. 1 and 2,

390

$$\frac{d[O(^1D)]}{dt} = k_{R3}[O_3] - k_{R4}[O(^1D)][H_2O] = 0, \qquad (1)$$

$$\frac{d[OH]}{dt} = 2k_{R4}[O(^1D)][H_2O] - k_{R1}[BVOC][OH] - k_{R2}[SO_2][OH] = 0, \qquad (2)$$

where k_{R1}, k_{R2}, k_{R3}, and k_{R4} are the rate constants referred to in Eqs. R1, R2, R3, and R4, respectively. Combining Eqs. 1 and

395 2, the rate of SO$_4^{2-}$(p) formation is described by Eq. 3, as follows,

$$\frac{d[SO_4^{2-}(p)]}{dt} = k_{R2}[SO_2][OH] = \frac{2k_{R2}k_{R3}[SO_2][O_3]}{k_{R1}[BVOC] + k_{R2}[SO_2]}. \qquad (3)$$

According to SAPRC-07 applied in the chemical transport model in this study, k_{R1} lies in the order ~10^{-11} cm^3 molecule^{-1} s^{-1}

400 and k_{R2} in the order of around ~10^{-13} cm^3 molecule^{-1} s^{-1}. The BVOC concentration is much higher than the SO$_2$ concentration in suburban and rural areas, meaning that k_{R1}[BVOC] is much higher than k_{R2}[SO$_2$]. Thus, Eq. 3 can be approximated into Eqs. 4, as follows,

$$r_{SO4} \equiv \frac{d[SO_4^{2-}(p)]}{dt} = k_{R2}[SO_2][OH] = \frac{2k_{R2}k_{R3}[SO_2][O_3]}{k_{R1}[BVOC]}. \qquad (4)$$

According to Eq. 4, the rate of $SO_4^{2-}(p)$ formation is proportional to O_3 and SO_2, and inversely proportional to BVOC. In terms of the chemical explanation, if BVOC emissions decrease due to changes in the UHI effect, the rate of reaction R1 is weakened and the redundant OH enhances reaction R2, which is why r_{SO4} is inversely proportional to BVOC. According to Fig. 5, mitigation of the UHI effect resulted in a decrease in O_3 within the S_{BVOC} scenario, which degraded the chemical reaction, and the decrease in BVOC was caused by mitigation of the UHI via the introduction of BEVs. Using Eq. 4, an increase in $SO_4^{2-}(p)$ occurs in the S_{BVOC} scenario compared with the BASE scenario when the decrease in O_3 is lower than the decrease in BVOC. Assuming all BVOC was isoprene (~70 % of BVOC emissions in Japan are isoprene (Hata et al., 2023)), the results of the ratio of r_{SO4} in BASE and S_{BVOC} ($\eta = r_{SO4}^{SBVOC}/r_{SO4}^{BASE}$) in daytime from 09:00 to 15:00 calculated by Eq. 4 are shown in Fig. 11(a). The η increases in the western and northern regions of GTA correspond to the distribution of the $SO_4^{2-}(p)$ increase described in Fig. 7. More qualitatively, the reduction in BVOC emissions reduces OH consumption, and the extra OH enhanced $SO_4^{2-}(p)$ formation in the western and northern regions of the GTA. Similarly, the decrease in primary emissions in the S_{EV} also leads to a decrease in the NO_X and VOCs emissions, which might enhance the $SO_2 + OH$ reaction, causing an increase in $SO_4^{2-}(p)$ and ultimately enhancing the formation of SOA (Sheehan and Bowman, 2001).

4.2.2 Sensitivity analysis of nighttime $PM_{2.5}$ changes

The photochemical reactions R3 and R4 do not occur during the night, as OH is generated from different sources. One of the well-known sources of OH at night is alkene ozonolysis, leading to the formation of Criegee intermediates (CIs), and both the vibrationally-excited and stabilized CIs form OH via unimolecular decomposition (Vereecken et al., 2017). These reaction pathways can be appended and described, as seen in reaction R5,

$$Alkene + O_3 \rightarrow vOH, \qquad (R5)$$
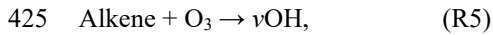
where v is a stoichiometric number that depends on the type of alkene. Alkenes also consume OH radicals via reaction R6, and the rates of OH consumption by alkenes are higher than those of other types of VOCs, such as alkanes and aromatics,

$$Alkene + OH \rightarrow SOA. \qquad (R6)$$
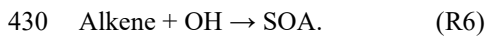
$SO_4^{2-}(p)$ is formed by reaction R2. Note that stabilized-CIs are also known to be strong oxidizers of SO_2 while the effect of $SO_4^{2-}(p)$ formation from stabilized CIs is almost negligible in the GTA (Nakamura et al., 2023). The steady-state approximation of the OH formation rate is given by Eq. 5,

$$\frac{d[OH]}{dt} = \nu k_{R5}[\text{Alkene}][O_3] - k_{R6}[\text{Alkene}][OH] - k_{R2}[SO_2][OH] = 0. \qquad (5)$$

where k_{R5} and k_{R6} are the rate constants of R5 and R6, respectively. Coupled with reaction R2, nighttime r_{SO4}, assuming simply that $\nu = 1$, is formulated as follows,

$$\frac{d[SO_4^{2-}(p)]}{dt} = k_{R2}[SO_2][OH] = \frac{2k_{R2}k_{R5}[\text{Alkene}][SO_2][O_3]}{k_{R1}[\text{Alkene}] + k_{R2}[SO_2]}. \qquad (6)$$

Assuming [Alkene] >> [SO$_2$] in the countryside, Eq. 6 can be transformed into Eq. 7 as follows,

$$r_{SO4} \equiv \frac{d[SO_4^{2-}(p)]}{dt} = k_{R2}[SO_2][OH] = \frac{2k_{R2}k_{R5}}{k_{R1}}[SO_2][O_3]. \qquad (7)$$

Therefore, nighttime r_{SO4} is directly proportional to the concentration of O$_3$. Chemically, nighttime alkene ozonolysis increases the number of OH radicals through CI-chemistry, indicating that O$_3$ concentration is the key factor involved in the OH concentration and r_{SO4}. The value of η (= $r_{SO4}^{SBVOC}/r_{SO4}^{BASE}$) in nighttime from 09:00 to 15:00 was calculated using Eq. 7, and the results are shown in Fig. 11(b). The fact that η takes a value of > 1.0 in central to northern regions of the GTA means that r_{SO4} will increase in S$_{BVOC}$ for most of the GTA. The increase in nighttime r_{SO4} is almost equivalent to the increase in daytime r_{SO4}, and r_{SO4} increases in the S$_{BVOC}$ scenario compared with BASE in both daytime and nighttime. As mentioned in Section 4.2.1, similar arguments can be made for the S$_{EV}$ scenario, where OH is treated as the source for the oxidation of alkenes. The nitrate radical (NO$_3$) that is formed by the reaction of NO$_2$ and O$_3$ is also known as an important oxidizer of alkenes at night (Ng et al., 2017). NO$_3$ adducts the C=C double bond of alkenes, finally forming organic peroxides (RO$_2$), which affect the nocturnal HO$_X$ cycle. For this reason, the reaction of alkenes with NO$_3$ is also expected to enhance OH formation and subsequent SO$_2$ oxidation; however, for simplicity, a discussion about NO$_3$ is omitted in this study. As shown in Section 4.2, mitigation of the UHI would cause an increase in SO$_4^{2-}$(p) and subsequent PM$_{2.5}$ formation; however, the change in the UHI affects BVOC emissions in the GTA, and the decrease in BVOC emissions also causes an increase in SO$_4^{2-}$(p) formation due to enhancement of the SO$_2$ + OH reaction.
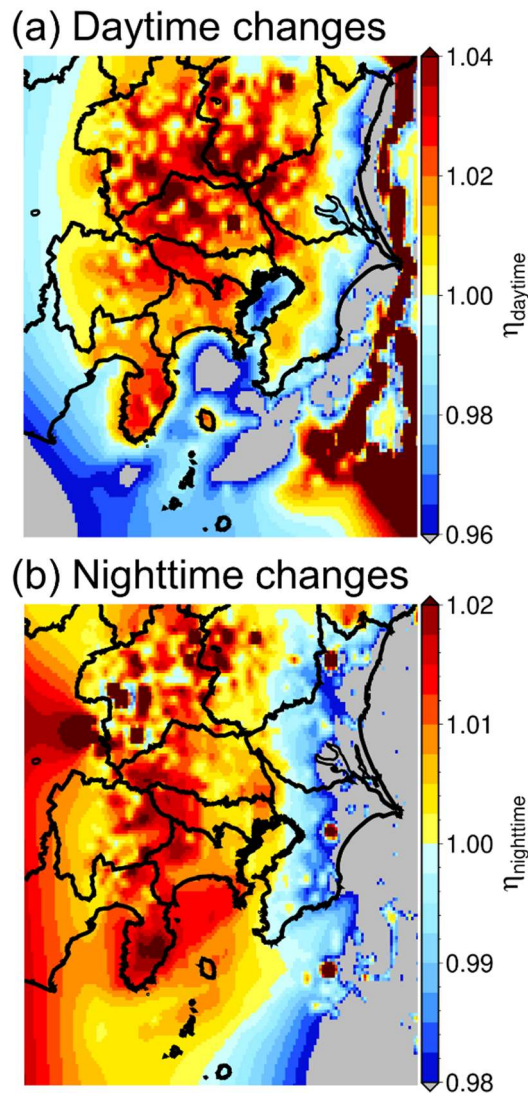
Figure 11: Annual mean ratio of the rate of sulfate formation (r_{SO4}), $\eta = r_{SO4}^{SBVOC}/r_{SO4}^{BASE}$, obtained by BASE scenario and S$_{BVOC}$ scenario for (a) daytime from 09:00 to 15:00 and (b) nighttime from 21:00 to 03:00.

4.3 Impact of introducing BEVs on premature mortality

465   Previous sections have suggested that introducing BEVs in the GTA will lead to an increase in O_3 in the urban area and an increase in $PM_{2.5}$ in the suburban/rural areas. To evaluate how these effects impact human health, we estimated the changes in premature mortality resulting from changes in O_3 and $PM_{2.5}$. The change in the number of deaths, ΔP, was calculated using Eq. 8, as follows,

$$\Delta P = \text{sgn}(\Delta C) \cdot \left(1 - e^{-\beta|\Delta C|}\right) \cdot P_d, \qquad (8)$$

where sgn is a sign function, ΔC is the change in concentration of air pollutants, P_d is the base number of deaths in the calculated region, and β is an epidemiological parameter that is defined by Eq. 9, as follows,

$$\beta = \frac{\ln(\text{RR})}{\Delta C_{\text{RR}}}, \qquad (9)$$

where RR is the relative risk from exposure to air pollutants, and ΔC_{RR} is the change in the concentration of a pollutant. Values of 1.003 for MDA8 O_3 change and 1.04 for daily average $PM_{2.5}$ with $\Delta C_{\text{RR}} = 10$ µg m^{-3} were used in this study (Poppe III et al., 2002; WHO Regional Office for Europe, 2008). The calculated target was the changes before and after the introduction of BEVs (the ALL scenario) for the entire GTA region (D3 in Fig. 1). The results show that there would be -175 fewer deaths caused by changes in the O_3 concentration (-1.41 × 10^{-4} % of the total population), while changes in the $PM_{2.5}$ concentration would lead to a decrease of -77 (-6.21 × 10^{-5} % of the total population), indicating that the number of deaths would decrease after the introduction of BEVs with respect to changes in both O_3 and $PM_{2.5}$. Premature mortality associated with changes in O_3 following the introduction of BEVs has been previously estimated for the urban part of the GTA; however, the study did not consider the effects in the rural area (Hata et al., 2019). According to the results of this study, O_3-related premature deaths over the entire GTA following the introduction of BEVs would save 175 lives in the region. However, $PM_{2.5}$ concentration increases are observed mainly in the suburban/rural areas due to changes in the kinetics of particle formation before and after the introduction of BEVs. However, as the population is condensed within the urban areas, where a decrease in $PM_{2.5}$ is estimated due to the decrease in primary emissions, the results show that 77 deaths would be prevented in the GTA. Therefore, according to the results of this study, the introduction of BEVs in the GTA would be effective, not only in supporting GHG emission issues but also for mitigating health impacts resulting from air pollution. The change in the UHI following the introduction of BEVs is one of the most important factors involved in changes in O_3 and $PM_{2.5}$. Nevertheless, it should be noted that in terms of $PM_{2.5}$, 102 more premature deaths are estimated for rural/suburban areas due to the increase in $PM_{2.5}$, mainly because of changes in the UHI and the increase in emissions from power plants, indicating that local health risks are likely to be induced by the introduction of BEVs.

4.4 Implications for policymaking

The introduction of BEVs as passenger vehicles to the market has been accelerated worldwide. In 2023, China ranked top in the BEV introduction rate (including plug-in hybrid vehicles) at 38%, followed by the European Union (21%), Israel (19%), and New Zealand (14%) (Global EV Data Explorer, 2024). However, in Japan, the BEV introduction rate was only 3.6% in 2023, although the national government has announced the complete substitution of new ICVs to BEVs in the market by 2030's. BEVs are expected to be dominant in Japan and worldwide in the future. According to the results of this study, the

introduction of BEVs to the GTA is estimated to be "totally" effective in mitigating O_3 and $PM_{2.5}$ pollution and related premature deaths. Despite these results, ground-level O_3 and $PM_{2.5}$ are expected to increase in some areas depending on the seasons and atmospheric conditions. This means that changes in O_3 and $PM_{2.5}$ should be carefully monitored at a local city level, not only with respect to the introduction of BEVs but also for all emission sources associated with emission reduction strategies. Positive effects are predicted to occur through the reduction in AH followed by the mitigation of UHI, which is a main focus of this study, and the total number of premature deaths caused by O_3 and $PM_{2.5}$ would be reduced. In addition, the decrease in AH and mitigation of the UHI would have a direct impact on reducing health issues, such as heatstroke. The number of deaths caused by heatstroke in the GTA was estimated at 128 in 2017 (Ministry of Health, Labour and Welfare of Japan, 2024); this value is compensated by the decrease in the number of premature deaths (252) attributed to secondary air pollution (175 by O_3 reduction and 77 by $PM_{2.5}$ reduction). Therefore, it is expected that introducing BEVs could mitigate the health impact in the GTA, and may possibly be as effective in other megacities worldwide.

4.5 Limitations and future perspectives

We found out the relationship between ground-level O_3 and $PM_{2.5}$ and mitigation of the UHI effect attributed to the introduction of BEVs in the GTA. Although our study provides new insights, it is of note that two assumptions were made in the setup of numerical simulations. First, the change in AH through introducing BEVs was assumed to be averagely distributed in the calculated region due to limitations in the parameterization of the UCM incorporated in the WRF. This assumption might have caused overestimations of the UHI effects in the countryside; however, as more than half of the area of the analyzed domain (D3) is composed of urban to suburban areas, the effect of overestimation is expected to be limited. Second, also because of the limitations of the parameterization of UCM, the increase in AH from power plants due to the increasing demand for battery charging was not considered. According to Section A.1 of the Appendix A, there would be a 34% increased energy demand for battery charging and the associated AH increase may not therefore be negligible. To account for these issues, it will be necessary to update the program for the UCM model incorporated in the WRF, and collaboration between developers of the WRF and scientists in the field of atmospheric science is recommended in future work.

5 Summary

The impacts of introducing BEVs on ground-level O_3 and $PM_{2.5}$ in the GTA were evaluated through chemical transport modeling, with a particular focus on the effect of the change in UHI. The results suggest O_3 increases in urban areas and $PM_{2.5}$ increases in suburban/rural areas that are dependent on regions and seasons. Changes in the UHI would contribute to a decrease in O_3 formation due to the degradation of O_3-related atmospheric chemistry (the increase in NO-titration effect and the degradation of photochemical reactions), while they would contribute to an increase in $PM_{2.5}$ due to the enhancement of particle condensation, and in some regions to a decrease in BVOCs, which would lead to enhanced $SO_4^{2-}(p)$ formation. The change in the number of annual premature deaths after introducing BEVs was calculated as 175 decreases in association with O_3 and 77

decreases for $PM_{2.5}$ over the entire GTA, suggesting positive impacts on human health. Previous studies have mainly focused on the effects of decreased primary emissions on ground-level O_3, due to the shift from ICVs to BEVs; however, no studies have shown clear evidence of how mitigation of the UHI through introducing BEVs has a local impact on O_3 and $PM_{2.5}$. This study shows the relevant impact of UHI mitigation on the decrease in O_3 and the increase in $PM_{2.5}$, for which absolute contributions were as high as the change in primary emissions. However, we only focused on road transportation, and future studies could focus on stationary sources and other transportation vehicles, such as ships, to clarify how electrification would change the local UHI effect, and subsequently affect air pollution. Finally, atmospheric data from 2017 were used in this study, but atmospheric conditions will change in the future when the entire transformation from ICVs to BEVs has occurred, such as in the 2050s; therefore, the O_3 formation sensitivity regime would also differ. Future research should therefore include emission inventories and meteorology for different time periods to comprehensively evaluate the effect of emission strategies and the UHI effect.

Appendix A: Estimation of the changes in anthropogenic heat as a result of converting ICVs to BEVs in 2017

A.1 Modelled vehicles and estimation of changes in exhaust emissions for the three types of vehicles and in emissions from power plants in the GTA

Tables A1 and A2 show the specifications of the modeled vehicles used to estimate changes in anthropogenic heat (AH) following vehicle substitution with BEVs. Three types of vehicles were compared in this study: light passenger cars, normal passenger cars, and small heavy-duty vehicles. Each type of vehicle was compared, and the same model was used for ICVs and BEVs, with differences involving the energy source (engine or battery). Based on the differences between ICVs and BEVs listed in Tables A1 and A2, change in AH were estimated as described in the following sentences.

Table A1: Specifications of passenger cars modeled in this study (L/100 km for internal combustion vehicles (ICVs) and Wh/km for battery electric vehicles (BEVs)).

Property	Light passenger car		Normal passenger car	
Category	ICV	BEV	ICV	BEV
Manufacturer	Nissan	Nissan	Toyota	Nissan
Model	SBA-B43W	ZAA-B6AW	BA-MZEA17W-AWXNB	ZAA-ZE1
Total weight (kg)	1060	1290	1535	1795
WLTC (L/100km and Wh/km)*	4.31	124	5.24	155
Urban (L/100km and Wh/km)*	5.15	100	7.35	133
Rural (L/100km and Wh/km)*	4.02	113	5.03	145
Highway (L/100km and Wh/km)*	4.15	142	4.46	171

Table A2: Specifications of small heavy-duty vehicles modeled in this study (L/100km for internal combustion vehicle (ICV) and Wh/km for battery electric vehicle (BEV)).

Property	Small heavy-duty vehicle	
	ICV	BEV
Category	ICV	BEV
Manufacturer	Mitsubishi	Mitsubishi
Model	2RG-FBAV0	ZAB-FEAVK
Total weight (kg)	4495	5015
JH25 (L/100km and Wh/km)*	8.46	347

The change in the emissions of primary air pollutants due to the substitution of ICVs with BEVs was estimated by multiplying the emission factors with the sources of engine exhaust emissions, evaporative emissions from vehicles (hot-soak loss, diurnal breathing loss, and running loss), and evaporative emissions from gasoline service stations as defined in the emission inventory provided by the Ministry of the Environment (Shibata and Morikawa, 2021). It was assumed that only light and normal passenger cars and small heavy-duty ICVs would be replaced with BEVs. The emissions from engine exhaust, evaporation from vehicles, and evaporation from service stations were set to zero by multiplying the emission factor of 0 by the emission inventories. The primary emissions of particles from brake and tire dust were not examined in this study.

The change in the emissions of primary air pollutants from power plants as a result of substituting ICVs with BEVs was estimated based on the catalog data of the three BEVs listed in Tables A1 and A2, statistical data of the number of vehicles in the GTA (Database from Automobile Inspection & Registration Information Association, 2024), and the average mileage per year (Ministry of Land, Infrastructure, Transport, and Tourism, 2024) listed in Table A3.

Table A3: Number of vehicles in GTA and the average mileage per year set in this study.

Category	Number of vehicles	Mileage (km/y)
Light passenger	11 286 521	10 575
Normal passenger	6 181 929	10 575
Small HV	3 053 453	14 325

Multiplying the number of vehicles in the GTA, mileage per year, and battery consumption listed in Tables A1 and A2 by the transmission loss of electricity from power plants to charging stations (1.038) resulted in a total energy demand of 49.6 TWh/y for charging BEVs in the GTA. The total energy demand for electricity in the GTA in 2017 was estimated at 147 TWh/y. Thus, the energy demand in power plants within the GTA after substituting ICVs with BEVs would increase by 49.6/147 × 100 = 34 %. We assumed that the increase in the primary emissions of air pollutants from power plants was proportional, at 34 %, in the BEV-introduction scenario.

A.2 Estimation of the change in anthropogenic heat (AH) for the three types of vehicles

580   The change in AH caused by substituting ICVs with BEVs was estimated for each vehicle type based on the energy efficiencies listed in Tables A1 and A2. The thermal enthalpies of gasoline (passenger cars) and light fuel (small heavy-duty vehicles) of ICVs were assumed to be 31250 kJ/L and 35770 kJ/L, respectively (Agency for Natural Resources and Energy, 2024), allowing the ratio of AH between the ICVs and BEVs to be calculated. For example, the fuel consumption of light passenger car ICV listed in Table A1 was 5.15 L/100 km. Multiplying the gasoline thermal enthalpy (31250 kJ/L by 5.15 L/100 km, resulted in a

585   total energy consumption of 1347 kJ/km. The battery consumption of the light passenger car BEV listed in Table A1 was 124 Wh/km = 446 kJ/km. Thus, the ratio of the decrease in AH caused by the introduction of light passenger BEVs was calculated at 446/1347 = 0.33. Similarly, the ratios of the decrease in AH by the introduction of BEV normal passenger cars and small heavy-duty vehicles were calculated at 0.34 and 0.41 respectively. By applying statistical data on the number of vehicles (Database from Automobile Inspection & Registration Information Association, 2024) listed in Table A3, the number-

590   weighted ratio of the decrease in AH was then calculated to be 0.35. This indicates that the change in AH before and after the introduction of BEVs contributed to the 35% decrease.

    The Ministry of the Environment released estimated data of UHI-related parameters, including AH, from stationery and transportation sources for the metropolitan area of Tokyo (Ministry of the Environment, 2010). According to this report, the AH from the transportation sector was 505.8 TJ/d, and the AH from all sectors was 1574.3 TJ/d. This study focused on the

595   electrification of passenger cars and small heavy-duty vehicles, and the ratio of the number of these vehicles in GTA was 89 %, meaning that the AH from the targeted vehicles was 505.8 × 0.892 = 451.5 TJ/d. The ratio of the decrease in the AH after the introduction of BEVs was calculated at 0.35; therefore, the decrease in AH after the introduction of BEVs would be 505.8 × 0.892 × 0.35 = 157.6 TJ/d, and the total AH from the vehicles after the introduction of BEVs in the transportation sector would be 505.8 – 451.5 + 157.6 = 211.9 TJ/d (the calculation of 505.8 - 451.5 corresponds to the AH from the non-targeted vehicles for electrification, and 157.6 corresponds to the AH from BEVs). The AH from all sectors after the introduction of BEVs was

600   calculated at 1574.3 – 505.8 + 211.9 = 1280.4 TJ/d. Finally, the ratio of the decrease in the total AH after the introduction of BEVs was calculated at 1280.4 / 1574.3 = 0.813. Therefore, a total decrease of 18.7 % (= (1.000 - 0.813) × 100) of AH is assumed for the GTA as a result of introducing BEVs under the assumptions made in these discussions.

Appendix B: Total emissions in the Greater Tokyo Area for the evaluated scenarios studied

605   Fig. B1 shows the annual total emissions of NO_X, CO, SO_2, and NH_3 in the four scenarios (BASE, ALL, S_{EV}, and S_{PP} defined in Table 1) in 2017 within the GTA (kt y^{-1}). While all the emissions would decrease due to the introduction of BEV (S_{EV}), the increased emissions from power plants would partly offset or increase total NO_X, CO, SO_2 (S_{PP}) emissions. The relevant decreases in NO_X (~20 %) and CO (~60 %) emissions are shown in ALL and S_{EV} scenarios.
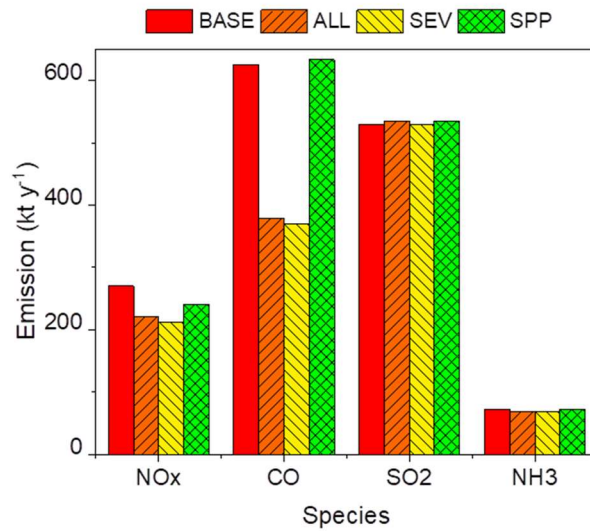
610 **Figure B1: Total annual NO$_X$, CO, SO$_2$, and NH$_3$ emissions in 2017 in the Greater Tokyo Area for the scenarios BASE, ALL, S$_{EV}$, and S$_{PP}$ listed in Table 1.**

Fig. B2 shows the total annual AVOC emissions for the four scenarios (BASE, ALL, S$_{EV}$, and S$_{PP}$, defined in Table 1) in 2017 within the GTA (kt y^{-1}). The species of "Others" in Fig. A2 include alcohols and acetylene. The decrease in AVOC emissions from BASE to ALL scenarios mainly relates to the decrease in exhaust and evaporative emissions from service stations;

615 however, the increase in emissions from power plants is almost negligible. A high decrease in alkane (~23 %) is expected in relation to the introduction of BEVs.
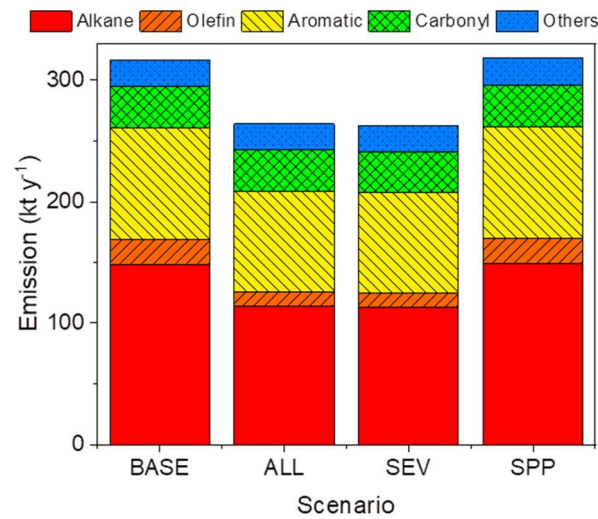
Figure B2: Total annual AVOC emissions in 2017 in the Greater Tokyo Area for the scenarios of BASE, ALL, S$_{EV}$, and S$_{PP}$ listed in Table 1.

Fig. B3 shows the total annual $PM_{2.5}$ emissions for the four scenarios (BASE, ALL, S_{EV}, and S_{PP}, defined in Table 1) in 2017 within the GTA (kt y^{-1}). Unlike NO_X, CO, and AVOCs, none of the $PM_{2.5}$ components show a relevant decrease following the introduction of BEVs. This means that the $PM_{2.5}$ emitted from vehicle exhaust emissions has almost no effect on total $PM_{2.5}$ emissions.
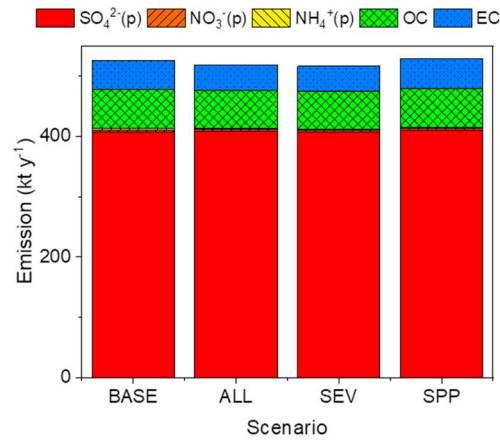
Figure B3: Total annual $PM_{2.5}$ emissions in 2017 in the Greater Tokyo Area for the scenarios of BASE, ALL, S_{EV}, and S_{PP} listed in Table 1. OC and EC are organic carbon and elemental carbon, respectively.

Fig. B4 shows the total annual BVOC emissions (isoprene and monoterpene) for the two scenarios (BASE and S_{BVOC}, defined in Table 1) in 2017 within the GTA (kt y^{-1}). The emissions in the two scenarios are almost equal, and only ~0.5 % of BVOC

 emissions decrease from the BASE to S_{BVOC} scenarios. This decrease was related to mitigation of the UHI effect through the introduction of BEVs.
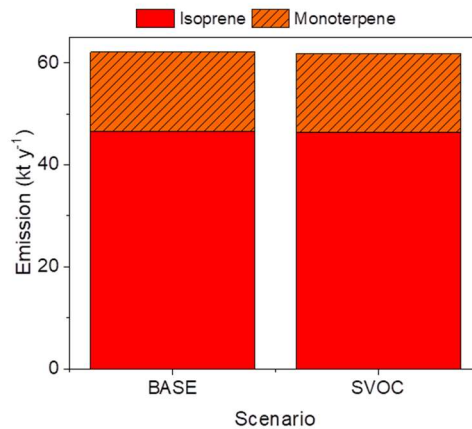
Figure B4: Total annual BVOC emissions in 2017 in the Greater Tokyo Area for the scenarios of BASE and S_{BVOC} listed in Table 1.

 Appendix C: Validation of simulated meteorology, O₃, and PM₂.₅ with the observed results

Figures C1–C4 show the correlation between observed and calculated results for the daily ground temperature, wind speed at 2-m height, wind direction, and total solar radiation for winter, spring, summer, and autumn in the seven analyzed sites in 2017. Note that the observed data of daily total solar radiation in Kanagawa, Chiba, Saitama, and Ibaraki were not available, so the remained three sites were compared. Furthermore, in terms of the wind direction shown in Fig. C3, the value was defined by the 16 directions: the value of 0 corresponds to 0° (north), 8 corresponds to 180° (south), and 15 corresponds to 337.5° (north-northwest). The correlations are exhibited using four statistical factors: correlation factor (R), root mean square error (RMSE), normalized mean bias (NMB), and normalized mean error (NME). Overall, the model was found to replicate the observed results well in all seasons. The results for the wind direction for Saitama and Tochigi show low R values of 0.19 and 0.29, respectively, but the time trend and the values of RMSE, NMB, and NME are similar to those of other sites. Unlike O₃ and PM₂.₅, there were no proposed indicators for the statistical values described in later sentences, but the time trend of simulated results shown in Figs. C1–C4 replicated the observed results, and we concluded that the simulated meteorology could be applied in the evaluation of this study.
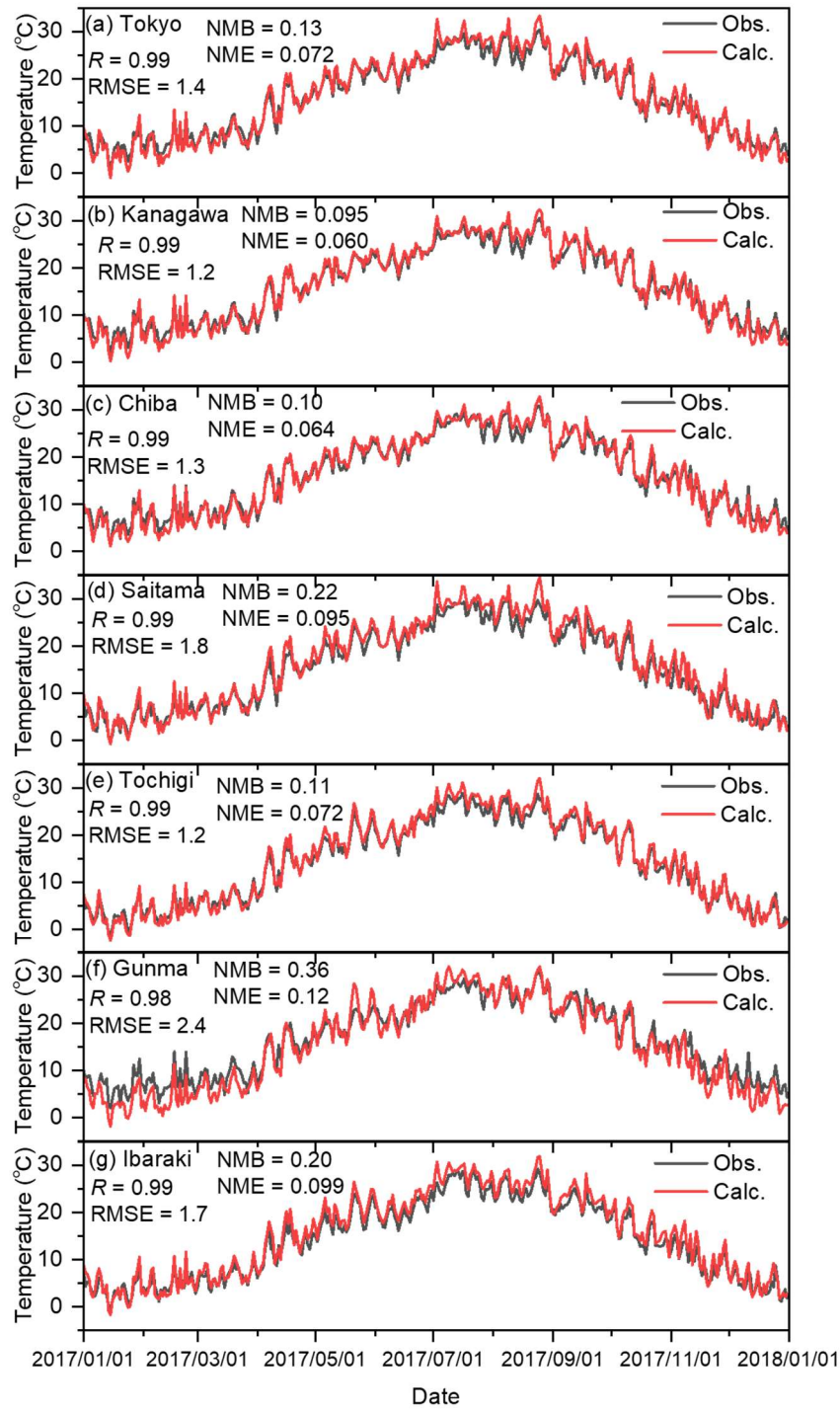
Figure C1: Comparison of observed (Obs.) and calculated (Calc.) daily averaged ground-temperatures in (a) Tokyo, (b) Kanagawa, (c) Chiba, (d) Saitama, (e) Tochigi, (f) Gunma, and (g) Ibaraki.

650
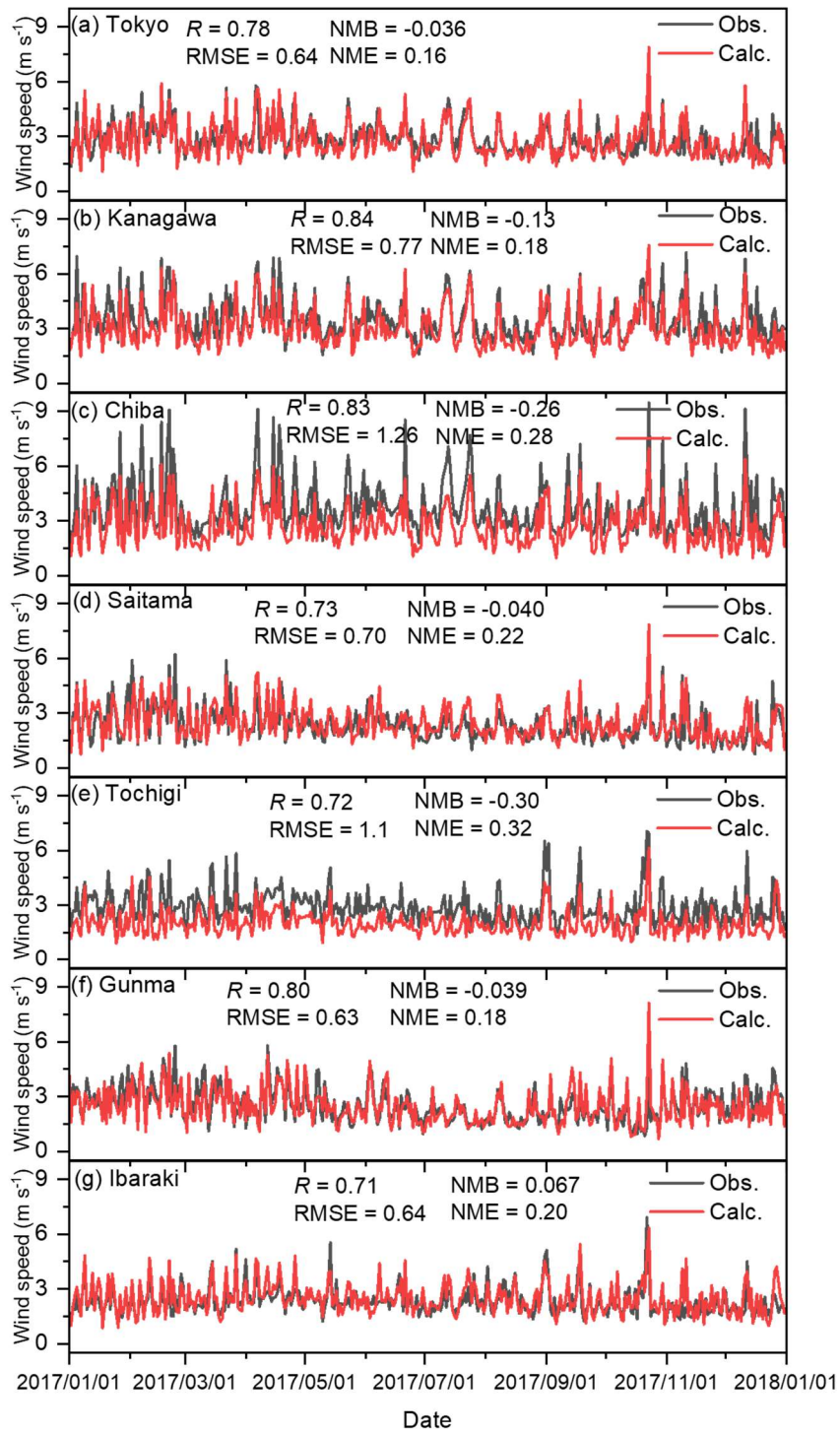
Figure C2: Comparison of observed (Obs.) and calculated (Calc.) daily averaged wind speeds in (a) Tokyo, (b) Kanagawa, (c) Chiba, (d) Saitama, (e) Tochigi, (f) Gunma, and (g) Ibaraki.
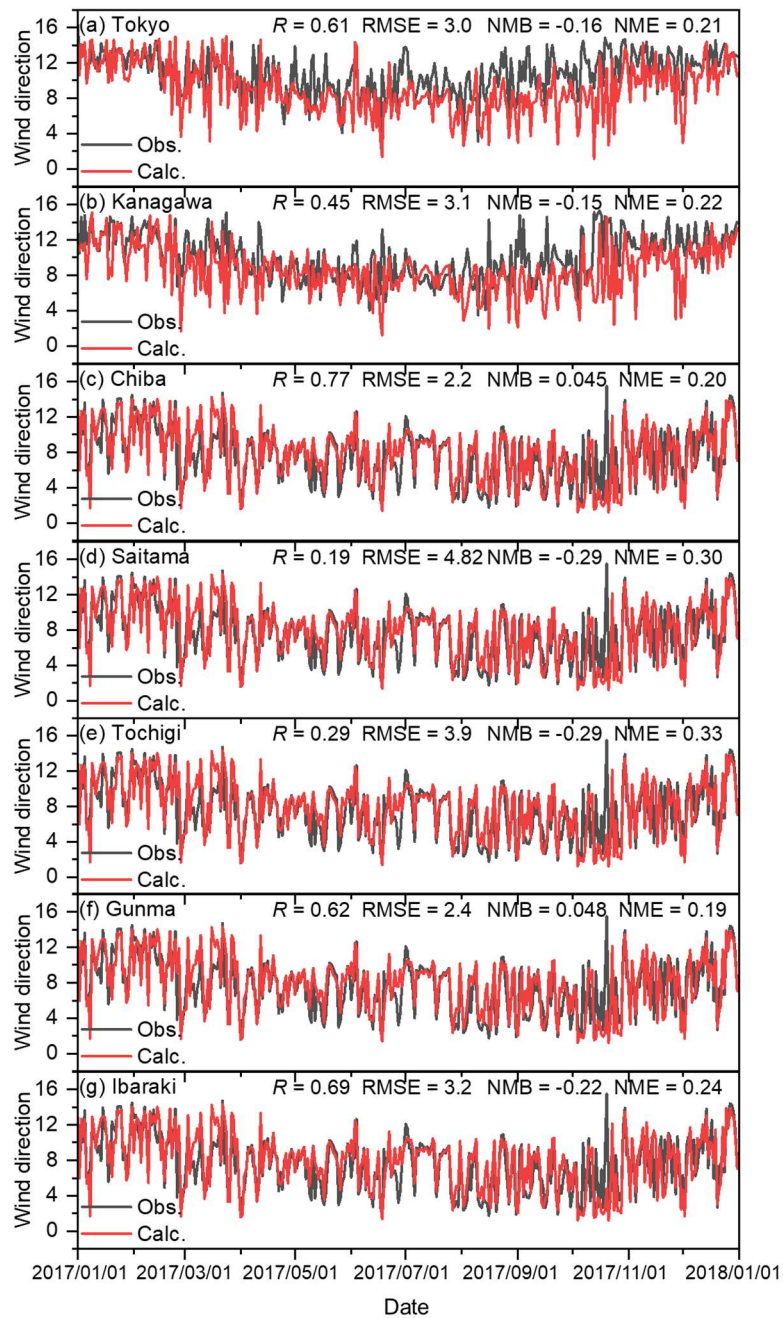
655

Figure C3: Comparison of observed (Obs.) and calculated (Calc.) daily averaged wind-directions in (a) Tokyo, (b) Kanagawa, (c) Chiba, (d) Saitama, (e) Tochigi, (f) Gunma, and (g) Ibaraki. Wind direction was defined by the 16 directions of which the value of 0 corresponds to 0° (north), 8 corresponds to 180° (south), and 15 corresponds to 337.5° (north-northwest).
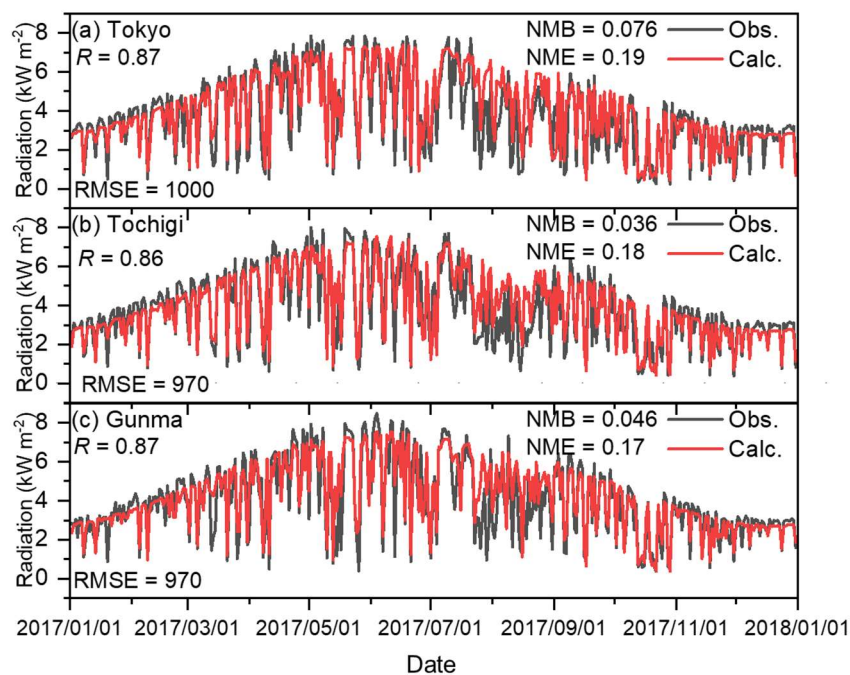
Figure C4: Comparison of observed (Obs.) and calculated (Calc.) daily total solar radiation in (a) Tokyo, (b) Tochigi, and (c) Gunma.

Figure C5 shows the correlation between the observed and calculated (BASE) results and 8-h daily maximum average (MDA8) O_3 concentrations. As seen in Fig. C5, overall, the modeled O_3 replicated the observed results well, and the R value was more than 0.7, except for that of Gunma. Figure C5(f) suggests a lower correlation for the modeled O_3 with the observed results for Gunma. Emery et al. proposed indicators that can be used to validate O_3 and $PM_{2.5}$ for chemical transport modeling (Emery et al., 2017). According to these indicators, the ideal values of the modeling performance for MDA8-O_3 should be $R > 0.75$, NMB < ±0.05, and NME < 0.15 while the criteria value should be $R > 0.50$, NMB < ±0.15, and NME < 0.25. All the sites except for Gunma fully met these criteria and were close to the described goals. However, Gunma did not meet the criteria for R and NME. This may be because it is located in the countryside, where less primary air pollutant emissions are generated than in highly polluted areas, and the transportation from other regions renders it difficult to predict O_3 by CTM. Nevertheless, most of calculations for the analyzed sites showed good agreements with the observed results, and are thus considered to be acceptable for analyzing this study. Fig. C6 shows the correlation between the observed and calculated (BASE) results of the 24-h daily average (DA24) $PM_{2.5}$ concentrations. Emery et al. proposed that ideal values of indicators used to the modeling performance of DA24 $PM_{2.5}$ should be $R > 0.70$, NMB < ±0.10, and NME < 0.35, while criteria should be $R > 0.40$, NMB < ±0.30, and NME < 0.50 (Emery et al., 2017). According to Fig. C6, all the modeled results except for those of Kanagawa met the criteria, and some R and NME values were close to the goal. The result of Kanagawa shown in Fig. C6(b) replicated the daily trend of the observed results. This analysis therefore shows that although relatively less accuracy was obtained for simulated $PM_{2.5}$ in Kanagawa, the modeled conditions could be applied in the analysis of this study.
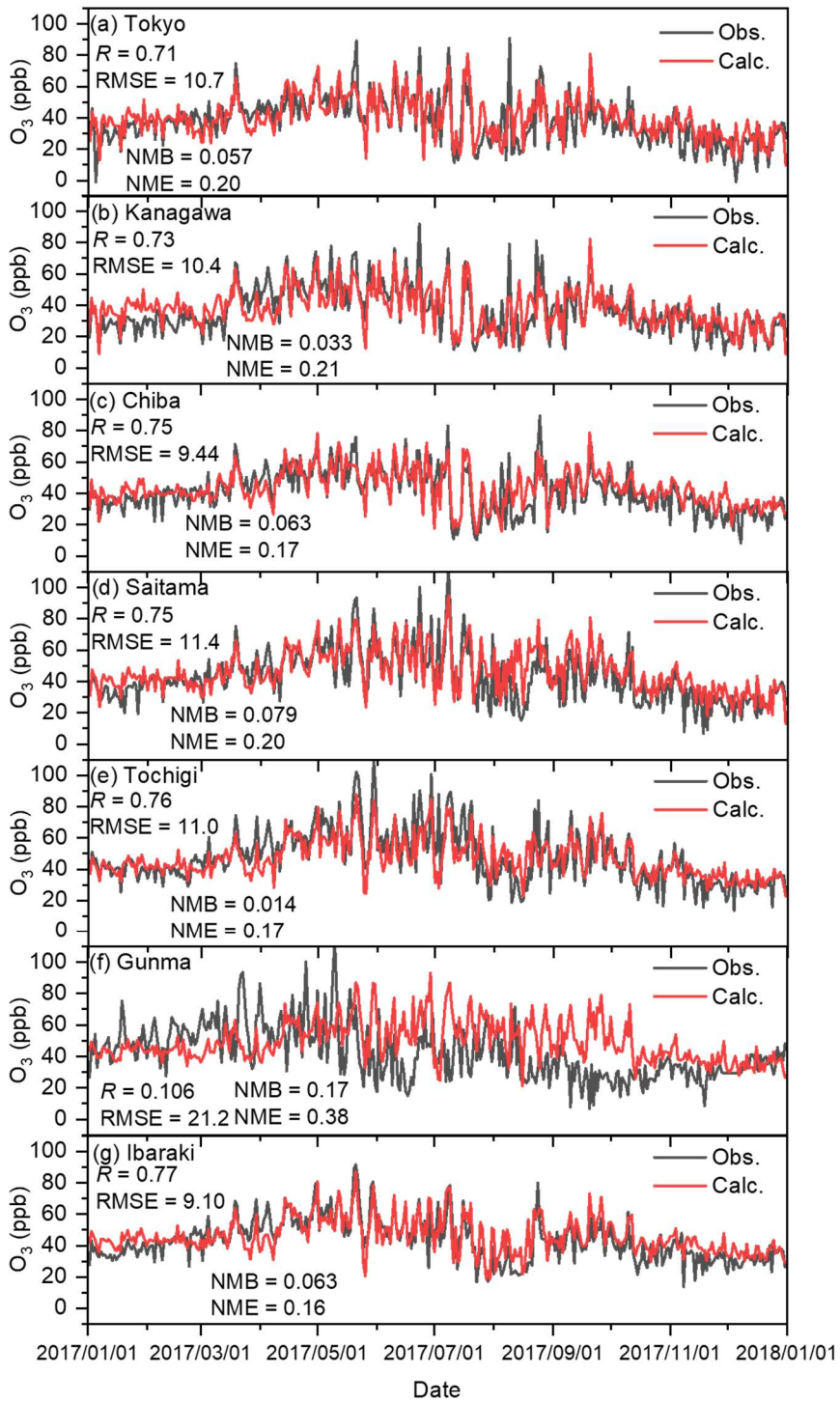
Figure C5: Comparison of observed (Obs.) and calculated (Calc.) 8-h maximum daily average O₃ concentrations in (a) Tokyo, (b) Kanagawa, (c) Chiba, (d) Saitama, (e) Tochigi, (f) Gunma, and (g) Ibaraki.

680
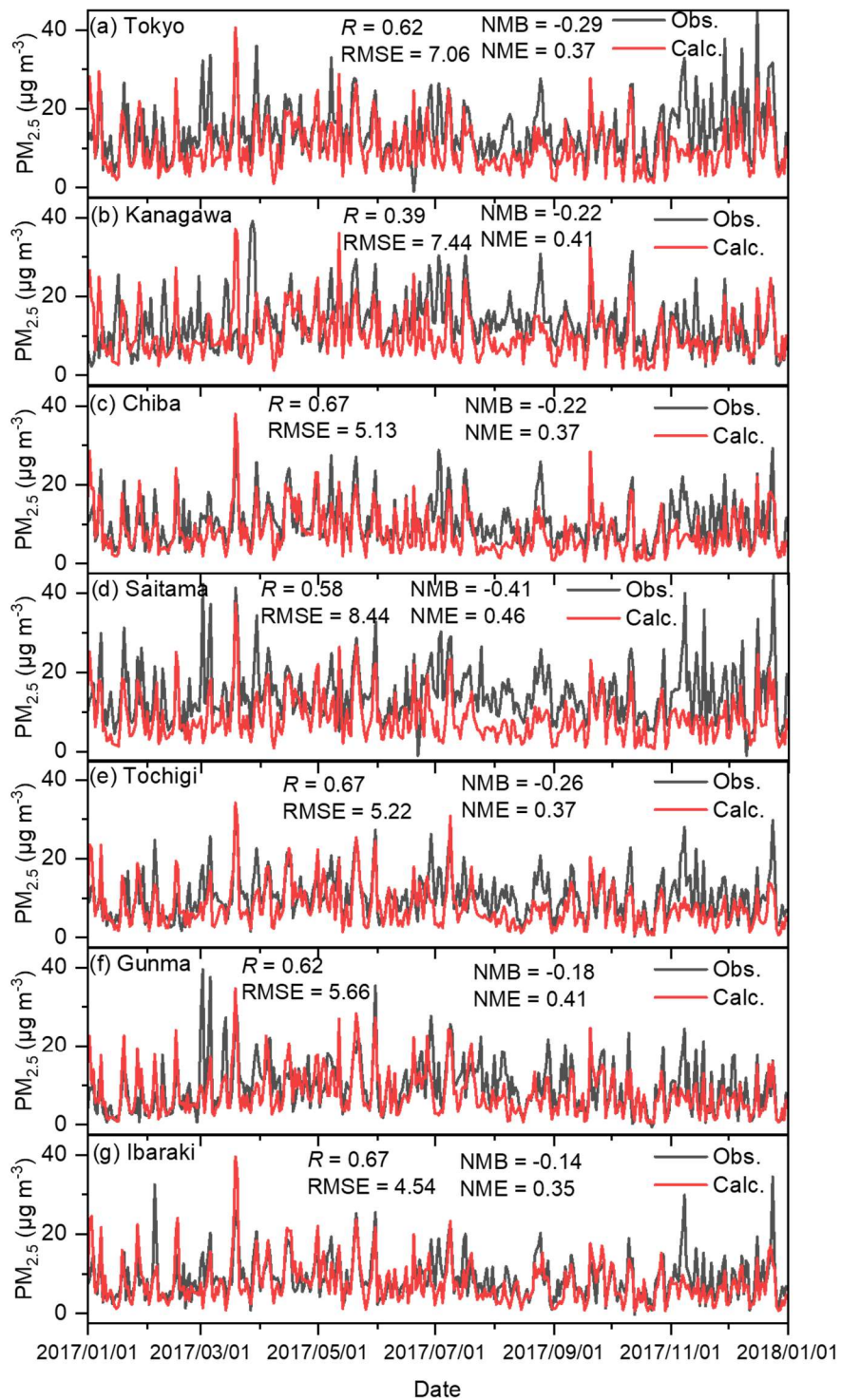
Figure C6: Comparison of observed (Obs.) and calculated (Calc.) daily average PM₂.₅ concentrations in (a) Tokyo, (b) Kanagawa, (c) Chiba, (d) Saitama, (e) Tochigi, (f) Gunma, and (g) Ibaraki.

Appendix D: Details of methods used to determine the ozone formation sensitivity regime

685   The formation of O_3 is dependent on the concentration of NO_X, and the rate of O_3 formation is determined by the concentration of VOCs. The balance of NO_X and VOCs concentrations thus determines whether O_3 formation is positive or negative when emission reduction strategies are implemented. Atmospheric conditions in high-NO_X regions, such as highly urbanized areas, are considered VOC-limited, while conditions in high-VOC regions such as forest, are NO_X-limited (Sillman, 1999). In the VOC-limited regime, the reduction in VOC emissions responded to a decrease in O_3 whereas the reduction in NO_X emissions

690   responded to an increase in O_3. In contrast, in the NO_X-limited regime, a reduction in the NO_X emissions corresponded to a decrease in O_3, with almost no response to VOC in terms of O_3 formation. Several indicators enabled the determination of the O_3-sensitivity regime in the targeted region. For example, the formaldehyde (HCHO) to NO_2 ratio (FNR) is commonly used to distinguish between VOC-sensitive (FNR < 1.0), NO_X-sensitive (FNR > 2.0), and transition regimes (1.0 ≤ FNR ≤ 2.0) (Tonnesen and Dennis, 2000; Martin et al., 2004; Duncan et al., 2010). The analytical hypothesis of the FNR relates to the fact

695   that HCHO is an intermediate product of atmospheric oxidation; thus, the amount of HCHO can be an indicator of VOCs. FNR has been commonly used in several studies; in particular, because of the availability of data on the column density of HCHO and NO_2 obtained from satellites such as the Ozone Monitoring Instrument (Vander, 2010) and TROPOspheric Monitoring Instrument (van Geffen et al., 2020). Nevertheless, HCHO is produced not only by the oxidation of VOCs, but also by primary emissions, and the value of the FNR strongly depends on the location (Jin et al., 2017). In addition to the FNR,

700   the hydrogen peroxide (H_2O_2) to HNO_3 ratio (HNR) has been proposed as an indicator of the ozone sensitivity regime (Sillman, 1995). The analytical hypothesis of the HNR was based on the fact that both H_2O_2 and HNO_3 are end products of the HO_X cycle and are produced via the termination reaction of two OH radicals to form H_2O_2 and the reaction of OH and NO_2 to form HNO_3. According to Kayaba et al., regimes are distinguished as VOC-sensitive (HNR < 0.5) and NO_X-sensitive (HNR > 0.5) in the GTA (Kayaba et al., 2023a). Unlike the FNR, the HNR does not directly depend on primary emissions; therefore, an

705   accurate analysis can be performed without considering location. Therefore, in this study, the HNR was used to discuss the O_3 sensitivity regime.

Data availability

All the data simulated data in this study are available upon request from the corresponding author.

Competing interests

710   The authors declare that they have no conflict of interest.

Acknowledgements

This study was supported by the Keidanren (Japan Business Federation) Foundation for Environmental Protection Measures. We thank Dr. Masayuki Hara at Kochi University for providing us with the urban canopy parameters for the WRF calculations. We also thank Dr. Yuya Takane of the National Institute of Advanced Industrial Science and Technology for the initial assistance with WRF calculations coupled with the urban canopy model. We also thank Dr. Kazuya Inoue at the National Institute of Advanced Industrial Science and Technology for his advice about the relationship between meteorology and ozone formation.

Author contributions

HH and TI proposed the research concept. NM calculated the energy consumption and anthropogenic heat from the data of conventional and electric vehicles. HH performed numerical simulations and analyses and drafted the manuscript. NM and TI reviewed the manuscript for accuracy.

References

Akimoto, H., Mori, Y., Sasaki, K., Nakanishi, H., Ohizumi, T., Itano, Y. Analysis of monitoring data of ground-level ozone in Japan for long-term trend during 1990–2010: Causes of temporal and spatial variation. Atmos. Environ., 102, 302–310, https://doi.org/10.1016/j.atmosenv.2014.12.001, 2015.

Agency for Natural Resources and Energy. Standard enthalpy and the emission factors of carbon dioxide from energy sectors. https://www.enecho.meti.go.jp/statistics/total_energy/pdf/stte_028.pdf (accessed April 19, 2024, in Japanese).

Andersson, Ö., Börjesson, Pal. The greenhouse gas emissions of an electrified vehicle combined with renewable fuels: Life cycle assessment and policy implications. Appl. Energy, 289, 116621, https://doi.org/10.1016/j.apenergy.2021.116621, 2021.

Binkowski, S.F.; Roselle, J.S. Models-3 community Multiscale Air Quality (CMAQ) model aerosol component 1. Model description. J. Geophys. Res. Atmos., 108(D6), 4183, https://doi.org/10.1029/2001JD001409, 2003.

Budisulistiorini, S.H., Nenes, A., Cariton, G.A., Surratt, J.D., McNeill, V.F., Pye, H.O.T. Simulating aqueous-phase isoprene-epoxydiol (IEPOX) secondary organic aerosol production during the 2013 Southern Oxidant and Aerosol Study (SOAS). Environ. Sci. Technol., 51(9), 5026–5034, https://doi.org/10.1021/acs.est.6b05750, 2017.

Carter, W.P.L. Development of the SAPRC-07 chemical mechanism. Atmos. Environ., 44(40), 5324–5335, https://doi.org/10.1016/j.atmosenv.2010.01.026, 2010.

Database from Automobile Inspection & Registration Information Association. https://airia.or.jp/ (accessed April 11, 2024, in Japanese).

740 Casals, C.L., Martinez-Laserna, E., Garcia, A.B., Nieto, N. Sustainability analysis of the electric vehicle use in Europe for CO_2 emissions reduction. J. Clean. Prod., 127, 425–437, https://doi.org/10.1016/j.jclepro.2016.03.120, 2016.

Chatani, S., Yamaji, K., Sakurai, T., Itahashi, S., Shimadera, H., Kitayama, K., Hayami, H. Overview of model inter-comparison in Japan's study for reference air quality modeling (J-STREAM). Atmosphere, 9(1), 19, https://doi.org/10.3390/atmos9010019, 2018.

745 Coates, J., Mar, K.A., Ojha, N. Butler, T.M. The influence of temperature on ozone production under varying NOx conditions - A modelling study. Atmos. Chem. Phys. 16, 11601–11615, 2016. https://doi.org/10.5194/acp-16-11601-2016.

Dubash, N.K., Khosla, R., Kelkar, U., Lele, S. India and climate change: evolving ideas and increasing policy engagement. Annu. Rev. Environ. Resour., 43, 395–424, https://doi.org/10.1146/annurev-environ-102017-025809, 2018.

Duncan, N.B., Yoshida, Y., Olson, R. J., Sillman, S., Martin, V.R., Lamsal, L., Hu, Y., Pickering, E.K., Retscher, C., Allen, 750 J.D., Crawford, H.J. Application of OMI observations to a space-based indicator of NO_X and VOC controls on surface ozone formation. Atmos. Environ., 44(18), 2213-2223, https://doi.org/10.1016/j.atmosenv.2010.03.010, 2010.

Emery, C., Liu, Z., Russell, G.A., Odman, T.M., Yarwood, G., Kumar, N. Recommendations on statistics and benchmarks to assess photochemical model performance. J. Air Waste Manag. Assoc., 67(5), 582–598, https://doi.org/10.1080/10962247.2016.1265027, 2017.

755 Fawzy, S., Osman, A.I., Doran, J., Rooney, D.W. Strategies for mitigation of climate change: a review. Environ. Chem. Lett., 18(6), 2069–2094, https://doi.org/10.1007/s10311-020-01059-w, 2020.

Ferero, E., Alessandrini, S., Balanzino, A. Impact of the electric vehicles on the air pollution from a highway. Appl. Energy, 169, 450–459, https://doi.org/10.1016/j.apenergy.2016.01.098, 2016.

Finlayson-Pitts, J.B., Pitts Jr. N.J. Atmospheric chemistry of tropospheric ozone formation: Scientific and regulatory 760 implications. Air & Waste, 43(8), 1091–1100, https://doi.org/10.1080/1073161X.1993.10467187, 1993.

Forrest, K., Kinnon, M.M., Tarroja, B., Samuelsen, S. Estimating the technical feasibility of fuel cell and battery electric vehicles for the medium and heavy duty sectors in California. Appl. Energy, 276, 115439, https://doi.org/10.1016/j.apenergy.2020.115439, 2020.

Fox, M., Zuidema, C., Bauman, B., Burke, T., Sheehan, M. Integrating public health into climate change policy and planning: 765 state of practice update. Int. J. Environ. Res. Public Health, 16(18), 3232, https://doi.org/10.3390/ijerph16183232, 2019.

Global EV Data Explorer. https://www.iea.org/data-and-statistics/data-tools/global-ev-data-explorer, 2024.

Gerasopoulos, E., Kazadzis, S., Vrekoussis, M., Kouvarakis, G., Liakakou, E., Kouremeti, N., Giannadaki, D., Kanakidou, M., Bohn, B., Mihalopoulos, N. Factors affecting O_3 and NO2 photolysis frequencies measured in the eastern Mediterranean during the five-year period 2002-2006. J. Geophys. Res. Atmos. 117 (D22), D22305, 2012. 770 https://doi.org/10.1029/2012JD017622.

Haman, L.C., Couzo, E., Flynn, H.J., Vizuete, W., Heffron, B., Lefer, L.B. Relationship between boundary layer heights and growth rates with ground-level ozone in Houston, Texas. J. Geophys. Atmos. 119, 6230-6245, 2014.

Hara, M., Kusaka, H., Kimura, F. Effect of global climate change on urban heat island intensity of Tokyo metropolitan area: winter season case. Nagare: Journal of Japan Society of Fluid Mechanics, 29(5), 353–361, 2010.

775 Hata, H., Tonokura, K. Impact of next-generation vehicles on tropospheric ozone estimated by chemical transport model in the Kanto region of Japan. Sci. Rep., 9, 3573, 2019.

Hata, H., Inoue, K., Kokuryo, K., Tonokura, K. Detailed inventory of the evaporative emissions from parked gasoline vehicles and an evaluation of their atmospheric impact in Japan. Environ. Sci. Technol., 54(10), 5947–5953, 2020.

Hata, H., Inoue, K., Yoshikado, H., Genchi, Y., Tsunemi, K. Impact of introducing net-zero carbon strategies on tropospheric
780 ozone (O_3) and fine particulate matter ($PM_{2.5}$) concentrations in Japanese region in 2050. Sci. Total Environ., 891, 164442, http://id.ndl.go.jp/bib/10905806, 2023.

Heidari, N., Pearce, J.M. A review of greenhouse gas emission liabilities as the value of renewable energy for mitigating lawsuits for climate change related damages. Renew. Sust. Energ. Rev., 55, 899–908, https://doi.org/10.1016/j.rser.2015.11.025, 2016.

785 Holmes, S.N. A review of particle formation events and growth in the atmosphere in the various environments and discussion of mechanistic implications. Atmos. Environ., 41(10), 2183–2201, https://doi.org/10.1016/j.atmosenv.2006.10.058, 2007.

Hosseinzadeh-Bandbafha, H., Rafiee, S., Mohammadi, P., Ghobadian, B., Lam, S.S., Tabatabaei, M., Aghbashlo, M. Exergetic, economic, and environmental life cycle assessment analyses of a heavy-duty tractor diesel engine fueled diesel-biodiesel-bioethanol blends. Energy Convers., 241, 114300, https://doi.org/10.1016/j.enconman.2021.114300, 2021.

790 Iacobuta, G., Dubash, N.K., Upadhya, P., Deribe, M., Höhne, N. National climate change mitigation legislation, strategy and targets: a global update. Clim. Policy, 18(9), 1114–1132, https://doi.org/10.1080/14693062.2018.1489772, 2018.

Itano, Y., Bandow, H., Takenaka, N., Saitoh, Y., Asayama, A., Fukuyama, J. Impact of NO_X reduction on long-term ozone trends in an urban atmosphere. Sci. Total Environ. 379, 46–55, https://doi.org/10.1016/j.scitotenv.2007.01.079, 2007.

Jin, X., Fiore, M.A., Murray, T.L., Valin, C.L., Lamsal, B., Duncan, K., De Smedt, I.B.F., Abad, G.G., Chance, K., Tonnesen,
795 S.G. Evaluating a space-based indicator of surface ozone-NOx-VOC sensitivity over midlatitude source regions and application to decadal Trends. J. Geophys. Res. Atmos., 122, 10439–10461, https://doi.org/10.1002/2017JD026720, 2017.

Kayaba, S., Kajino, M. Potential impact of battery electric vehicle penetration and changes in upstream process emissions assuming night-charging on summer O_3 concentration in Japan. J. Geophys. Res. Atmos., 128(11), e2022JD037578, https://doi.org/10.1029/2022JD037578, 2023a.

800 Kayaba, S., Kajino, M. Potential impacts of energy and vehicle transformation through 2050 on oxidative stress-inducing $PM_{2.5}$ metals concentration in Japan. GeoHealth, 7(10), e2023GH000789, 2023b. https://doi.org/10.1029/2023GH000789.

Japan Meteorological Agency archives. https://www.jma.go.jp/jma/indexe.html (accessed April 11, 2024).

Kusaka, H., Kondo, H., Kikegawa, Y., Kimura, F. A simple single-layer urban canopy model for atmospheric models: Comparison with multi-layer and slab models. Boundary Layer Meteorol., 101, 329–358,
805 https://doi.org/10.1023/A:1019207923078, 2001.

Li, C., Cao, Y., Zhang, Mi., Wang, J., Liu, J., Shi, H., Geng, Y. Hidden benefits of electric vehicles for addressing climate change. Sci. Rep., 5, 9213, https://doi.org/10.1038/srep09213, 2015.

Li, N., Chen, J.-P., Tsai, I-C., He, Q., Chi, S.-Y., Lin, Y.-C., Fu, T.-M. Potential impacts of electric vehicles on air quality in Taiwan. Sci. Total Environ. 566-567, 919–928, https://doi.org/10.1016/j.scitotenv.2016.05.105, 2016.

810 Lin, W.-Y., Hsiao, M.-C., Wu, P.-C., Fu, S.J., Lai, L.-W., Lai, H.-C. Analysis of air quality and health co-benefits regarding electric vehicle promotion coupled with power plant emissions. J. Clean. Prod. 247, 119152, https://doi.org/10.1016/j.jclepro.2019.119152, 2020.

Marin, V.R., Fiore, M.A., Van Donkelaar, A. Space-based diagnosis of surface ozone sensitivity to anthropogenic emissions. Geophys. Res. Lett., 31(6), https://doi.org/10.1029/2004GL019416, 2004.

815 Meng, X., Jiang, J., Chen, T., Zhang, Z., Lu, B., Liu, C., Xue, L., Chen, J., Herrmann, H., Li, X. Chemical drivers of ozone change in extreme temperatures in eastern China. Sci. Total Environ. 874, 16424, 2023. https://doi.org/10.1016/j.scitotenv.2023.162424.

Ministry of Health, Labour and Welfare of Japan, Demographic statistics from 2013 to 2020. https://www.mhlw.go.jp/stf/english/index.html (accessed September 30, 2024).

820 Ministry of Land, Infrastructure, Transport, and Tourism. Data of the actual use of road transportation. https://www.mlit.go.jp/jidosha/iinkai/seibi/5th/5-2.pdf (accessed April 11, 2024, in Japanese).

Ministry of the Environment. Inventory of urban anthropogenic heat. https://www.env.go.jp/air/report/h16-05/chpt01.pdf (accessed April 11, 2024, in Japanese).

Morino, Y., Kondo, Y., Takegawa, N., Miyazaki, Y., Kita, K., Komazaki, Y., Fukuda, M., Miyakawa, T., Moteki, N., Worsnop, 825 R.D. Partitioning of HNO_3 and particulate nitrate over Tokyo: Effect of vertical mixing. J. Geophys. Res. Atmos., 111, D15215, https://doi.org/10.1029/2005JD006887, 2006.

Moro, A., Lonza, L. Electricity carbon intensity in European Member States: Impacts on GHG emissions of electric vehicles. Transp. Res. D Transp. Environ., 64, 5–14, https://doi.org/10.1016/j.trd.2017.07.012, 2018.

Mulrow, J., Grubert, E. Greenhouse gas emissions embodied in electric vehicle charging infrastructure: a method and case 830 study of Georgia, US 2021-2050. Enriron. Res.: Infrastruct. Sustain., 3, 015013, https://doi.org.10.1088/2634-4505/acc548, 2023.

Muratori, M. Impact of uncoordinated plug-in electric vehicle charging on residential power demand. Nat. Energy, 3, 193–201, https://doi.org/10.1038/s41560-017-0074-z, 2018.

Murphy, B.N., Nolt, G.C., Sidi. F, Bash, O.J., Appel, W.K, Jang, C., Kang, D., Kelly, J., Mathur, R., Napelenok, S., Pouliot, 835 G., Pye, T.O.H. The detailed emissions scaling, isolation, and diagnostic (DESID) module in the community multiscale air quality (CMAQ) modeling system version 5.3.2. Geosci. Model Dev., 14, 3407–3420, https://doi.org/10.5194/gmd-14-3407-2021, 2021.

Nakamura, Y., Hata, H., Tonokura, K. Urban-scale analysis of the seasonal trend of stabilized-Criegee intermediates and their effect on sulphate formation in the Greater Tokyo Area. Environ. Sci.: Atmos., 3, 1758–1766, https://doi.org/10.1039/D3EA00105A, 2023.

National Center for Atmospheric Research archives. NCEP FNL Operational Model Global Tropospheric Analyses, continuing from July 1999. 10.5065/D6M043C6 (accessed April 11, 2024).

National Oceanic and Atmospheric Administration. Environmental Modeling Center archives. https://polar.ncep.noaa.gov/sst/ (accessed April 11, 2024).

Ng, L.N.; Brown, S.S., Archibald, T.A., Atlas, E., Cohen, C.R., Crowley, N.J., Day, A.D., Donahue, M.N., Fry, L.J., Fuchs, H., Griffin, J.R., Guzman, I.M., Herrmann, H., Hodzic, A., Iinuma, Y., Jimenez, L.J., Kiendler-Scharr, A., Lee, H.B, Luecken, J.D., Mao, J., McLaren, R., Mutzel, A., Osthoff, D.H., Ouyang, B., Picquet-Varrault, B., Platt, U., Pye, T.O.H., Yinon Rudich, Y., Schwantes, H.R., Shiraiwa, M., Stutz, J., Thornton, A.J., Tilgner, A., Williams, J.B., Zaveri, A.R. Nitrate radicals and biogenic volatile organic compounds: oxidation, mechanisms, and organic aerosol. Atmos. Chem. Phys., 17, 2103–2162, https://doi.org/10.5194/acp-17-2103-2017, 2017.

Nuruzzaman, M. Urban heat island: Causes, effects and mitigation measures – A review. IJEMA, 3(2), 67–73, https://doi.org/10.11648/j.ijema.20150302.15, 2015.

Pan, S., Roy, A., Choi, Y., Eslami, E., Thomas, S., Jiang, X., Gao, O.H. Potential impacts of electric vehicles on air quality and health endpoints in the Greater Houston Area in 2040. Atmos. Environ. 207, 38–51, https://doi.org/10.1016/j.atmosenv.2019.03.022, 2019.

Poppe III, A.C., Burnett, T.R., Thun, J.M. Lung cancer, cardiopulmonary mortality, and long-term exposure to fine particulate air pollution. JAMA., 287(9), 1132–1141, https://doi.org/10.1001/jama.287.9.1132, 2002.

Requia, J.W., Mohamed, M., Higgins, D.C., Arain, A., Ferguson, M. How clean are electric vehicles? Evidence-based review of the effects of electric mobility on air polutants, greenhouse gas emissions and human health. Atmos. Environ., 185, 64–77, https://doi.org/10.1016/j.atmosenv.2018.04.040, 2018.

Rizvi, A.H.S., Agrawal, P., Batra, S., Nidhi, N., Singh, V. Assessing urban heat island intensity and emissions with compressed natural gas in non-commercial vehicles. Urb. Clim., 48, 101421, https://doi.org/10.1016/j.uclim.2023.101421, 2023.

Rosenfeld, H.A., Akbari, H., Romm, J. J., Pomeranz, M. Cool communities: strategies for heat island mitigation and smog reduction. Energy Build., 28(1), 51–62, https://doi.org/10.1016/S0378-7788(97)00063-7, 1998.

Schreyer, F., Luderer, G., Rodrigues, R., Pietzcker, R.C., Baumstark, L. Sugiyama, M., Brecha, R.J., Ueckerdt, F. Common but differentiated leadership: strategies and challenges for carbon neutrality by 2050 across industrialized economies. Environ. Res. Lett., 15(11), 114016, https://doi.org/10.1088/1748-9326/abb852, 2020.

Santiago, V.J., Inoue, K., Tonokura, K. Modeling ground ozone concentration changes after variations in precursor emissions and assessing their benefits in the Kanto region of Japan. Atmosphere, 13(8), 1187, https://doi.org/10.3390/atmos13081187, 2022.

Sheehan, E.P., Bowman, M.F. Estimated effects of temperature on secondary organic aerosol concentrations. Environ. Sci. Technol., 35(11), 2129–2135, https://doi.org/10.1021/es001547g, 2001.

Shen, W., Han, W., Wallington, J.T., Winkler, L.S. China electricity generation greenhouse gas emission intensity in 2030: Implications for electric vehicles. Environ. Sci. Technol., 53(10), 6063–6072, https://doi.org/10.1021/acs.est.8b05264, 2019.

Shibata, Y., Morikawa, T. Review of the JCAP/JATOP air quality model study in Japan. Atmosphere, 12 (8), 943, https://doi.org/10.3390/atmos12080943, 2021.

Sillman, S. The use of NO_y, H_2O_2, and HNO_3 as indicators for ozone- NO_X-hydrocarbon sensitivity in urban locations. J. Geophys. Res., 100(D7), 14175–14188, https://doi.org/10.1029/94JD02953, 1995.

Sillman, S. The relation between ozone, NO_X and hydrocarbons in urban and polluted rural environments. Atmos. Environ., 33(12), 1821–1845, https://doi.org/10.1016/S1352-2310(98)00345-8, 1999.

Skamarock, W.C., Klemp, J.B., Dudhia, J., Gill, D.O., Barker, D.M. Duda, M.G., Huang, X.-Y., Wang, W., Powers, J.G. A description of the advanced research WRF version 4. NCAR Technical Note. http://pfigshare-u-files.s3.amazonaws.com/14057147/WRF_TechNote_Jan2019.pdf (accessed April 11, 2024).

Soet, A., Guevara, M., Baldasano, M.J. The potential impacts of electric vehicles on air quality in the urban areas of Barcelona and Madrid (Spain). Atmos. Environ., 99, 51–63, https://doi.org/10.1016/j.atmosenv.2014.09.048, 2014.

Stathopoulou, E., Mihalakakou, G., Santamouris, M., Bagiorgas, S.H. On the impact of temperature on tropospheric ozone concentration levels in urban environments. J. Earth Syst. Sci., 117, 227–236, https://doi.org/10.1007/s12040-008-0027-9, 2008.

Strapason, A., Woods, J., Pérez-Cirera, V., Elizondo, A., Cruz-Cano, D., Pestiaux, J., Cornet, M., Chaturvedi, R. Modelling carbon mitigation pathways by 2050: insights from the global calculator. Energy Strategy Rev., 29, 100494, https://doi.org/10.1016/j.esr.2020.100494, 2020.

Tonnesen, G.S., Dennis, R.L. Analysis of radical propagation efficiency to assess ozone sensitivity to hydrocarbons and NO_X: 2. Long-lived species as indicators of ozone concentration sensitivity. J. Geophys. Res., 105(D7), 9227–9241, https://doi.org/10.1029/1999JD900372, 2000.

Ulpiani, G. On the linkage between urban heat island and urban pollution island: Three-decade literature review towards a conceptual framework. Sci. Total Environ. 751, 141727, https://doi.org/10.1016/j.scitotenv.2020.141727, 2021.

Vander, A.R. Tropospheric emission monitoring internet service. https://www.temis.nl/index.php (Accessed May 21, 2024)

van Geffen, J., Oersma, F.K., Eskes, H., Sneep, M., ter Linden, M., Zara, M., Veefkind, P.J. S5P TROPOMI NO2 slant column retrieval: method, stability, uncertainties and comparisons with OMI. Atmos. Meas. Tech., 13, 1315–1335, https://doi.org/10.5194/amt-13-1315-2020, 2020.

Vereecken, L., Novelli, A., Taraborrelli, D. Unimolecular decay strongly limits the atmospheric impact of Criegee intermediates. Phys. Chem. Chem. Phys., 19, 31599–31612, https://doi.org/10.1039/C7CP05541B, 2017.

905 Volkamer, R., Jimenez, L.J. Martini, S.F., Dzepina, K., Zhang, Q., Salcedo, D., Molina, T.L., Worsnop. R.D., Molina, J.M. Secondary organic aerosol formation from anthropogenic air pollution: Rapid and higher than expected. Geo. Phys. Lett., 33(17), L17811, https://doi.org/10.1029/2006GL026899, 2006.

Wang, Y., Du, H., Xu, Y., Lu, D., Wang, X., Guo, Z. Temporal and spatial variation relationship and influence factors on surface urban heat island and ozone pollution in the Yangtze River Delta, China. Sci. Total Environ., 631-632, 921–933, https://doi.org/10.1016/j.scitotenv.2018.03.050, 2018.

910 Warneke, C., de Gouw, A.J., Goldan, D.P., Kuster, C.W., Williams, J.E. Lerner, M.B., Jakoubek, R., Brown, S.S., Stark, H., Aldener, M., Ravishankara, A.R., Roberts, M.J., Marchewka, M., Bertman, S., Sueper, T.D., McKeen, A.S., Meagher, F.J., Fehsenfeld, C.F. Comparison of daytime and nighttime oxidation of biogenic and anthropogenic VOCs along the New England coast in summer during New England Air Quality Study 2002. J. Geophys. Res. Atmos., 109(D10), https://doi.org/10.1029/2003JD004424, 2004.

915 WHO Regional Office for Europe, Copenhagen. Health risks of ozone from long-range transboundary air pollution. 2008. ISBN: 9789289042895.

Xie, M., Zhu, K, Wang, T, Feng, W, Gao, D, Li, M, Li, S., Zhuang, B., Han, Y., Chen, P., Liao, J. Changes in regional meteorology induced by anthropogenic heat and their impacts on air quality in South China. Atmos. Chem. Phys., 16, 15011–15031, https://doi.org/10.5194/acp-16-15011-2016, 2016.

920 Yamada, H., Inomata, S., Tanimoto, H., Hata, H., Tonokura, K. Estimation of refueling emissions based on theoretical model and effects of E10 fuel on refueling and evaporative emissions from gasoline cars. Sci. Total Environ., 622–623, 467–473, https://doi.org/10.1016/j.scitotenv.2017.11.339, 2018.